Review Article

Characterization of Cellulose*

Fumio TANAKA**

(Accepted November 16, 1985)

CONTENTS

* This article is based on the Ph. D. thesis written by the auther. The title of the thesis is "Orientation and Texture of Cellulose Crystallites in *Pinus densiflora* Wood".

** Research Section of Wood Chemistry.

GENERAL INTRODUCTION

Wood is consisted of a large number of lignificated cell walls (Shimaji *et al.* 1976). From chemical point of view, it is composed of cellulose, lignin, hemicellulose and a small amount of many kinds of extractives (Migita *et al.* 1968; Fujii *et al.* 1982). Among these wood components, the wood cellulose is a linear natural polymer, and most parts of which are in crystalline state. The wood lignin is a nonlinear heterogeneous three-dimensional polymer, and is in amorphous state in contrast to the wood cellulose. Some hemicelluloses are linear like wood cellulose, and the other have branchings in their molecular structures. They are usually

less crystalline. The wood extractives are generally low molecular weight compounds, and constitute small portion of wood components. From anatomical point of view, wood is consisted of two kinds of cellar units, one is derived from fusiform initials and the other from parenchyma cells. The former have the function of tracheae for water, holding wood body, and so on. The latter have the function of storing nutritious substances (Migita *et al.* 1968).

Among woody plants the structural constitutions of softwood are simpler than hardwood. About 90% parts of softwood elements are tracheids, which are derived from fusiform cambium cells. Therefore, it is natural to consider that the physical properties of softwood depend largely on the physical properties of the tracheids.

The tracheid is mainly consisted of primary and secondary walls. The former is formed when the tracheid is derived from the cambium cell, and the latter is formed after the primary wall formation is completed, and the tracheid grows its thickness during the secondary wall formation. The secondary wall is generally consisted of three layers named S_1, S_2 and S_3 layers. There are transition areas among these layers. The S_2 layer is the most abundant among these layers. It has, therefore, been considered that the properties of tracheid depend largely on those of this layer. The influence of other layers on the physical properties of the tracheid is relatively small.

The each layer of tracheids is considered as a "sheet" which is consisted of many fibrilar units called microfibrils. From the study on the relations between the physical properties of wood and its structural units, it was found that many properties of wood were generally influenced by the orientation of microfibrils in a "sheet" (Norimoto *et al.* 1981). The physical properties of wood, then can be evaluated quantitatively if the properties of microfibrils and their orientation distributions are known.

The properties of microfibrils can be characterized by the properties of cellulose crystallites and the orientations, because microfibrils are fine fibrils constructed with cellulose crystallites. Orientation of cellulose crystallites in microfibrils, however, can not be measured directly, because of their fine fibrilar form. It is, therefore, difficult to explain some characteristics of microfibrils on the basis of those of cellulose crystallites, although the bulk properties of wood can be explained on the basis of the characteristics for cellulose crystallites, because cellulose crystallites orientations for whole wood can be easily obtained directly by some conventional technique. In order to explain the bulk properties of wood on the basis of cellulose crystallites, it is sufficient that three dimensional orientation distributions of cellulose crystallites in wood are obtained, as well as the properties of wood cellulose. The purpose of this investigation is a characterization of wood cellulose, and an evaluation of orientation distributions of wood cellulose.

There have been many studies on cellulose crystallites orientation in wood in which the cellulose is treated as one of the polycrystalline materials. Direct observation with optical microscope (Wardrop 1954, Harada *et al.* 1985), birefringence (Preston 1952, Wardrop 1954) and x-ray diffraction (Preston 1952, Wardrop 1954, Okano 1972, Nitta *et al.* 1973) were used in these studies. These studies, however, did not explain whole features of cellulose crystallites orientations in wood, but only an averaged feature of orientation in a selected region of orientation distributions.

Although the direct observation with optical microscope is a suitable method for the observation of orientational features in the size of microfibrils, it can not show the orientations of three main crystallographic axes of cellulose crystatllites in wood, because cellulose crystallites in wood are very small, and can not be seen by this technique directly. Thus the method is not useful for the orientation study of cellulose crystallites in wood. The birefringence method is an excellent one, because one can get the orientations of amorphous cellulose chains as well as cellulose crystallites. It, however, is not practical, because it is difficult to evaluate the form birefringence in observed data. The x-ray diffraction method is, on the contrary, useful in the study on the orientations of cellulose crystallites although it does not respond to the cellulose chain in the amorphous region. By the use of x-ray diffraction method it is easy to get the crystalline scatterings in the observed scatterings and collect the informations only from the crystalline regions. As some kind of physical properties of wood was affected by those of cellulose crystallites, the x-ray diffraction method was applied in this study in order to get some information on the orientation and texture of cellulose crystallite in wood.

There are two techniques in measurement of orientations of crystallites with x-ray diffraction method: one is on the basis of x-ray photographic technique, and the other is on the basis of x-ray diffractometry. The former has unavoidable technical defects in the measurements which will be explained later. Therefore, the x-ray diffractometry was applied in these studies. To measure the crystallite orientations by diffractometry, ploe figure analysis is popular in the field of the texture study of metals (Cullity 1956). Cellulose crystallites in wood, however, are clearly different from metal crystallites in sizes, and in degrees of perfection of crystallites. They are different in interactions which are caused by x-ray, the magnitude of background scatterings for x-ray diffraction, and so on. So the pole figure technique can not be directly applied in the study on the orientation of wood cellulose. The technique was modified so as to be applicable in this study, and the modified pole figure method was first applied to *Valonia* cellulose as a model specimen, and the validity of this modification was confirmed. The technique was further modified in order to be fully available for wood cellulose. Applying the modified pole figure

method to *Pinus densiflora* wood, three-dimensional orientation distributions of cellulose crystallites were evaluated, and the wood cellulose was also characterized. From these studies, the deviation of wood cellulose from naturally occurring other celluloses was discussed.

THEORY AND EXPERIMENTALS FOR X-RAY DIFFRACTION

1. X-ray diffraction from single crystals

1-1. X-ray diffraction from a crystal

As was shown in Fig. 1, x-ray scattering from crystals can be considered as a simple reflection on the lattice planes. The equation (1) is obtained between the incident and the diffracted x-rays, when the lattice plane coincide with the xy-plane in Fig. 1,

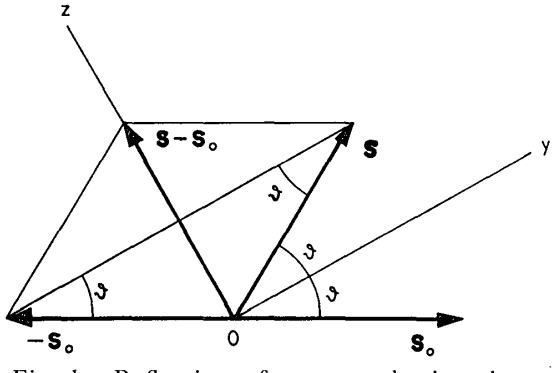

Fig. 1. Reflection of x-ray on lattice plane.

$$|\boldsymbol{s}-\boldsymbol{s}_0| = 2\sin\frac{\chi}{2} = 2\sin\theta \qquad (1)$$

where $\boldsymbol{s}$ and $\boldsymbol{s}_0$ are unit vectors on the incident and the diffracted x-rays, and χ ($=2\theta$, θ: Bragg angle) is a scattering angle. This equation can be explained geome-

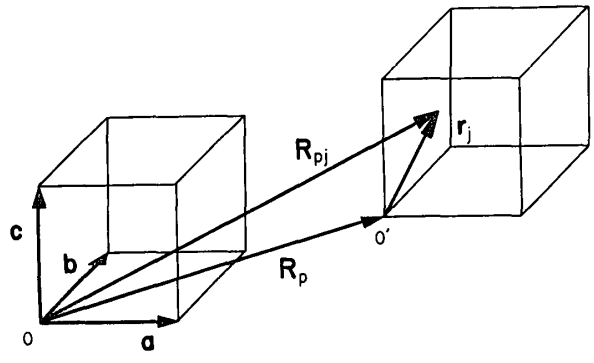

Fig. 2. Positional vector for j-th atom in (p, q, r) unit cell.

trically, assuming a reflection to be observed only in the condition that the all scattering x-rays are in phase. In order to describe the diffraction phenomenon precisely, the secondary waves from all parts of materials should be considered (Vainshtein 1963). The position of a j-th atom in an unit cell at an arbitrary position of (p, q, r) is, then, considered (Fig. 2). The position vector from the origin $\boldsymbol{O}$ against the origin $\boldsymbol{O}_p$ at the position (p, q, r) is $\boldsymbol{R}_p$ and that from $\boldsymbol{O}_p$ against j-th atom in the unit cell is $\boldsymbol{r}_j$, and the following equations are obtained,

$$\boldsymbol{R}_p = p\boldsymbol{a} + q\boldsymbol{b} + r\boldsymbol{c} \tag{2}$$

$$\boldsymbol{r}_j = x_j\boldsymbol{a} + y_j\boldsymbol{b} + z_j\boldsymbol{c} \tag{3}$$

where $\boldsymbol{a}$, $\boldsymbol{b}$ and $\boldsymbol{c}$ are the unit vectors on the three main crystallographic axes (a, b and c axes), p, q and r are the coordinates of an origin $\boldsymbol{O}_p$ for a unit cell in the crystal lattice space, and x_j, y_j and z_j are the coordinates of the j-th atom against the origin $\boldsymbol{O}_p$ of the unit cell. The position vector $\boldsymbol{R}_{pj}$ for the j-th atom against the origin $\boldsymbol{O}$ is, then, shown as follows.

$$\begin{aligned}\boldsymbol{R}_{pj} &= \boldsymbol{R}_p + \boldsymbol{r}_j \\ &= (p+x_j)\boldsymbol{a} + (q+y_j)\boldsymbol{b} + (r+z_j)\boldsymbol{c}\end{aligned} \tag{4}$$

The path difference between secondary waves, which are diffracted with this j-th atom and the origin $\boldsymbol{O}$, is described by the Eq. (5), as is shown in Fig. 3.

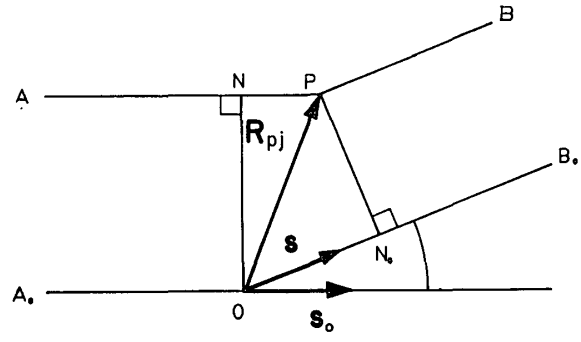

Fig. 3. Path differences between x-rays diffracted at points $\boldsymbol{O}$ and $\boldsymbol{P}$.

$$\begin{aligned}\Delta_{pj} &= \boldsymbol{ON}_0 - \boldsymbol{PN} \\ &= (\boldsymbol{R}_{pj}\boldsymbol{s}) - (\boldsymbol{R}_{pj}\boldsymbol{s}_0) \\ &= \boldsymbol{R}_{pj}(\boldsymbol{s} - \boldsymbol{s}_0)\end{aligned} \tag{5}$$

The phase of the secondary wave for the path $\boldsymbol{APB}$ is shifted in front of that for $\boldsymbol{A}_0\boldsymbol{OB}_0$ by the path difference Δ_{pj}.

The amplitude of secondary waves scattered by j-th atom is shown by the Eq. (6),

$$\phi_j = \sqrt{I_e} f_j \exp\left[\frac{2\pi i}{\lambda}\{\boldsymbol{R}_{pj}(\boldsymbol{s} - \boldsymbol{s}_0)\}\right] \tag{6}$$

where I_e is the scattering intensity for one electron, f_j is the number of electrons for the j-th atom, and i is an imaginary unit. The value of I_e is given by the Eq. (7),

$$I_e = I_0 \frac{e^4}{m^2c^4} \frac{1}{r^2} \frac{\{1+\cos^2(2\chi)\}}{2} \tag{7}$$

where I_0 is an intensity for nonpolarized incident x-ray, e is an electric element, m is a mass of an electron, c is a speed of x-ray beam, and r is a distance from the scattering center to an observing point.

The amplitude of secondary waves for the whole crystal is described in the Eq. (8) as the sum of the amplitudes for secondary waves from all unit cells in the crystal.

$$\Psi = \sqrt{I_e} \sum_p \sum_q \sum_r \sum_j f_j \exp\left[\frac{2\pi i}{\lambda}\{\boldsymbol{R}_{pj}(\boldsymbol{s}-\boldsymbol{s}_0)\}\right] \tag{8}$$

Using the reciprocal vector $\boldsymbol{a}^*$, $\boldsymbol{b}^*$ and $\boldsymbol{c}^*$ with the coefficients ξ, η and ζ defined as follows (Eq. 9).

$$\begin{aligned}(\boldsymbol{s}-\boldsymbol{s}_0)\boldsymbol{a} &= \xi\lambda \\ (\boldsymbol{s}-\boldsymbol{s}_0)\boldsymbol{b} &= \eta\lambda \\ (\boldsymbol{s}-\boldsymbol{s}_0)\boldsymbol{c} &= \zeta\lambda\end{aligned} \tag{9}$$

$(\boldsymbol{s}-\boldsymbol{s}_0)/\lambda$ can be expressed as follows (Eq. 10).

$$\frac{(\boldsymbol{s}-\boldsymbol{s}_0)}{\lambda} = \xi\boldsymbol{a}^* + \eta\boldsymbol{b}^* + \zeta\boldsymbol{c}^* \tag{10}$$

Substituting the Eq. (8) by the Eq. (10), the equation (11) is obtained.

$$\Psi = \sqrt{I_e} \sum_p \sum_q \sum_r \sum_j f_j \exp\{2\pi i(p\xi - q\eta + r\zeta + x_j\xi + y_j\eta + z_j\zeta)\} \tag{11}$$

The equation (12) is also obtained from the Eqs. (1) and (10).

$$\frac{4\sin^2\theta}{2} = |\xi\boldsymbol{a}^* + \eta\boldsymbol{b}^* + \zeta\boldsymbol{c}^*|^2 \tag{12}$$

As every unit cell has generally the same arrangement of atoms in the crystal, there is the common term in the Eq. (11), as shown in the Eq. (13),

$$F(\xi, \eta, \zeta) = \sum_j f_j \exp\{2\pi i(\xi x_j + \eta y_j + \zeta z_j)\} \tag{13}$$

where $F(\xi, \eta, \zeta)$ is called the structure factor or the structure amplitude. Thus, the equation (13) can be converted into the Eq. (14).

$$\Psi = \sqrt{I_e} F(\xi, \eta, \zeta) \sum_p \sum_q \sum_r \exp\{2\pi i(p\xi + q\eta + r\zeta)\} \tag{14}$$

In order to calculate the amplitude of secondary waves for whole crystal, a parallelepiped is considered which have three kind of edges whose length are $L \times |\boldsymbol{a}|$, $M \times |\boldsymbol{b}|$ and $N \times |\boldsymbol{c}|$, respectively. In order to simplify this discussion, the sum for the amplitude of the secondary waves becomes independent of the terms p, q and r, assuming that the crystal form factor can be disregarded. The equation (14) is converted into the Eq. (15).

$$\Psi = \sqrt{I_e}\, F(\xi, \eta, \zeta) \sum_{p=0}^{L-1} \exp(2\pi i p\xi) \sum_{q=0}^{M-1} \exp(2\pi i q\eta) \sum_{r=0}^{N-1} \exp(2\pi i r\zeta)$$

$$= \sqrt{I_e}\, F(\xi, \eta, \zeta) \frac{\sin \pi L\xi}{\sin \pi\xi} \frac{\sin \pi M\eta}{\sin \pi\eta} \frac{\sin \pi N\zeta}{\sin \pi\zeta}$$

$$\exp[\pi i\{(L-1)\xi + (M-1)\eta + (N-1)\zeta\}] \qquad (15)$$

The intensity of the diffraction, $I(\xi, \eta, \zeta)$, is described as Eq. (16).

$$I(\xi, \eta, \zeta) = \Psi\Psi^*$$

$$= I_e F(\xi, \eta, \zeta) F^*(\xi, \eta, \zeta) \frac{\sin^2 \pi L\xi}{\sin^2 \pi\xi} \frac{\sin^2 \pi M\eta}{\sin^2 \pi\eta} \frac{\sin^2 \pi N\zeta}{\sin^2 \pi\zeta} \qquad (16)$$

The trigonometric terms in the Eq. (16) are specially called "Laue function" (Eq. 17),

$$\text{Laue}\ (L, M, N, \xi, \eta, \zeta) = \frac{\sin^2 \pi L\xi}{\sin^2 \pi\xi} \frac{\sin^2 \pi M\eta}{\sin^2 \pi\eta} \frac{\sin^2 \pi N\zeta}{\sin^2 \pi\zeta} \qquad (17)$$

which has the maximum value under the condition of Eq. (18).

$$\xi = h,\ \eta = k,\ \text{and}\ \zeta = l \quad (h, k, l: 0, 1, 2, \ldots) \qquad (18)$$

The maximum value of the Laue function is, then, given as follows (Eq. 19).

$$\text{Laue}_{\max.}(L, M, N, \xi, \eta, \zeta) = L^2M^2N^2 \qquad (19)$$

The values of the Laue functions (Eq. 19) are very small and negligible when the values of L, M, and N are large enough except for the condition $\xi = h$, $\eta = k$ and $\zeta = l$ (Eq. 18). Under the condition $\xi = h$, $\eta = k$ and $\zeta = l$, the equation (9) becomes as follows,

$$\begin{aligned} (\boldsymbol{s} - \boldsymbol{s}_0)\boldsymbol{a} &= h\lambda \\ (\boldsymbol{s} - \boldsymbol{s}_0)\boldsymbol{b} &= k\lambda \\ (\boldsymbol{s} - \boldsymbol{s}_0)\boldsymbol{c} &= l\lambda \end{aligned} \qquad (20)$$

The maximum intensity of the diffraction is observed, when the path differences of scattered x-rays along three direction $\boldsymbol{a}$, $\boldsymbol{b}$ and $\boldsymbol{c}$ are integral multiple values of the wave length of the incident x-ray. The equation (20) is called "Laue condition", and the coefficients h, k and l "Laue order".

1-2. Ewald's shpere and Bragg's condition of reflection

Equation (21) is obtained, when Laue condition (Eq. 20) is described in vector expression.

$$\frac{\boldsymbol{s} - \boldsymbol{s}_0}{\lambda} = h\boldsymbol{a}^* + k\boldsymbol{b}^* + l\boldsymbol{c}^* = \boldsymbol{h} \qquad (21)$$

The equation (22) is obtained from the Eq. (21) as shown in Fig. 4.

$$\boldsymbol{OH} = \boldsymbol{OA} + \boldsymbol{AH} = \frac{-\boldsymbol{s}_0}{\lambda} + \frac{\boldsymbol{s}}{\lambda} = \boldsymbol{h} \qquad (22)$$

The sphere with the raidus of $1/\lambda$ around the point $\boldsymbol{A}$ in Fig. 4 is called the "Ewald's sphere of reflection". It is clear from Fig. 4 that the reciprocal lattice point $\boldsymbol{H}$ for the lattice plane (hkl) is on the Ewald's sphere when this point $\boldsymbol{H}$ is under the Laue condition, and vice versa. Equations (23) and (24) can be derived from the geomet-

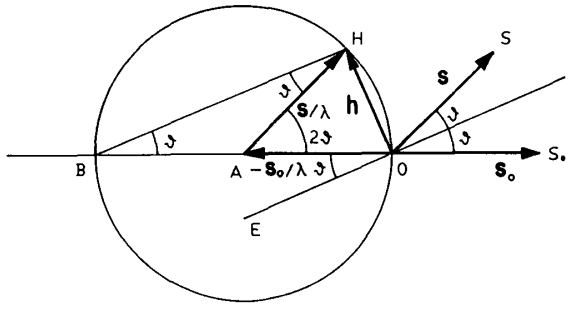

Fig. 4. Schematic representation of Laue condition and Ewald's sphere.

rical relationships shown in Fig. 4 where d is an interplanar spacing between the lattice plane (hkl),

$$OH = OB \sin\theta = \frac{2}{\lambda} \sin\theta \tag{23}$$

$$OH = |\boldsymbol{OH}| = |\boldsymbol{h}| = \frac{1}{d} \tag{24}$$

and the following equation is obtained.

$$2d \sin\theta = \lambda \tag{25}$$

The equation (25) is the "Bragg's condition of reflection".

2. Relationship between the orientations of the lattice planes of crystallites in polycrystalline materials and the Ewald's sphere

The orientation distributions of the reciprocal vectors $\boldsymbol{h}_{hkl}$, each of which is corresponding to a lattice plane (hkl) in the crystallite, are able to be described in the distribution map around the point $\boldsymbol{O}$ in Fig. 4, and the distributions are equivalent to the orientation distributions of the lattice planes (hkl). Considering a sphere with the raidus $r = |\boldsymbol{h}_{hkl}| = 1/d_{hkl}$ around the point $\boldsymbol{O}$ in Fig. 4, which is called "reference sphere", the orientation distributions of lattice planes (hkl) can be described with the distributions for the points on the tops of the reciprocal vectors $\boldsymbol{h}_{hkl}$ that are located on the reference sphere. Then, the orientation distributions for the lattice plane (hkl) can be obtained, if the distributions of these points on the reference sphere is known (Cullity 1956).

Now the reciprocal vector shown in Fig. 5 is considered under the Laue condition. Only the vectors are available which have the tops on the intersection for both reference and Ewald's spheres: the reference circle. This means that the diffraction patterns obtained with the incident x-ray from one direction corresponds to only the distributions on this reflection circle, which is the cross sectional feature of the distribution on reference sphere. Many x-ray diffraction patterns from different directions of incident x-ray are, therefore, necessary in order to obtain the

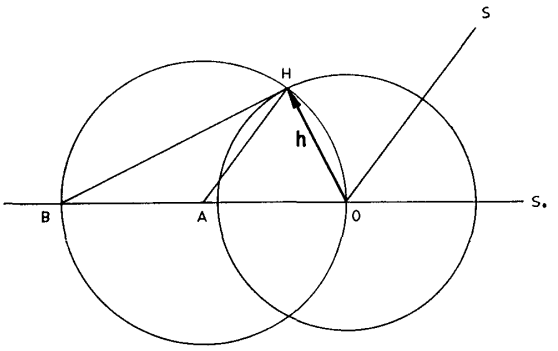

Fig. 5. Schematic representation of Laue condition.

distribution for all reciprocal vectors (*hkl*). Therefore, the specimen should be rotated three dimensionally against the incident x-ray beam, and the diffraction patterns have to be obtained at each sample geometry.

3. Degree of crystallinity for Macromolecules

3-1. X-ray Diffraction of Macromolecules

X-ray diffraction patterns from amorphous materials having poor ordered internal structure are diffuse and are called a "hallo", while those from crystalline materials having well-ordered internal structure are intense and discrete. This means that one can identify the internal structure of materials by measuring x-ray diffraction intensity (Alexander 1969). The x-ray diffraction method is also applicable to polymers. Polymers show two kind of x-ray diffraction patterns: one is the intense and discrete, and the other is diffuse hallo. This means that polymers are consisted of two type regions of different internal structure: crystalline region and noncrystalline region. This is known as the "two phase model concept". Based on the concept, the degree of crystallinity defined as weight percent of crystalline region in the total weight of a polymer has been used as an index to characterize the polymeric materials.

However, the structure of polymers is complicated and seems not to be explained by this two phase model concept. It is uncertain whether there are clear border lines between crystalline and noncrystalline regions. Disordered regions might by present even in the crystalline regions. The two phase model concept has become inadequate to express the polymer sturcture. Instead, the paracrystalline model concept is proposed by Hosemann (1967) to explain new observations. Her concept does not distinguish crystalline regions from noncrystalline regions. In this concept, the degree of orderedness for internal structure of polymers is changing continuously, and there is no clear border line between crystalline and noncrystalline regions.

Some workers insist that the degree of crystallinity has lost its theoretical background and that the values of degree of crystallinity become meaningless. Although the paracrystalline model concept is a general one, I think that the two phase model concept can be applied as an approximate estimation. Furthermore, the values of degree of crystallinity for polymers have good correlations with the physical properties of polymers phenomenologically (Alexander 1969). Thus, the degree of crystallinity can be considered to reflect the internal structures of polymers to a certain degree. Therefore, in some case, the degree of crystallinity is useful to evaluate the structure of macromolecular substances.

3-2. Degree of Crystallinity

The degree of crystallinity is defined as a ratio of the diffraction intensity of the crystallites to that of whole sample, and expressed as Eq. (26).

$$D.C.=\frac{I_{\mathrm{cry.}}(2\theta)\,d(2\theta)}{I_{\mathrm{total}}(2\theta)\,d(2\theta)} \tag{26}$$

To calculate the *D.C.* value it is necessary to separate the scatterings for crystalline regions from total scattering. From the two phase model concept, it is shown that the total scattering is the sum of both crystalline and noncrystalline scattering. The crystalline scattering is intense and discrete, and the noncrystalline scattering is broad and diffuse. If this diffuse scattering is taken off from the total scattering, the crystalline scattering is obtained. In practice, however, this diffuse scattering patterns can not be evaluated unless a perfect amorphous sample from the same material is prepared. Usually it is difficult to obtain an amorphous sample of natural ploymers, especially of cellulose. The evaluation of amorphous scattering, then should be achieved with a method to avoid the contingent error in the process.

4. Size of crystallites

It is clear from the Eq. (16) that the line broadening of diffraction peak has a close correlation with the crystalline sizes, that is L, M and N values. Scherrer (1918), who used a Gaussian equation (27) instead of Laue function (Eq. 17), derived the Eq. (28),

$$\mathrm{Laue}\ (L, M, N, \xi, \eta, \zeta)=L^2M^2N^2\exp\{-(L^2\xi^2+M^2\eta^2+N^2\zeta^2)\} \tag{27}$$

$$D_{hkl}=\frac{0.94\lambda}{\beta_0\cos\theta} \tag{28}$$

where D_{hkl} is the dimension of crystallite in the direction of the reciprocal vector [***hkl***], β_0 is the half breadth of pure line profile of (hkl) peak in radian, λ is the wave length of the incident x-ray, and θ is the Bragg angle of (hkl) diffraction. The value β_0 is obtained from the observed line profile when it is corrected for the effect of line broadening by instrument used (Jones 1938). For more detailed analysis,

it is not sufficient to use above β_0 value, because the pure line profile also includes the effect of line broadenings caused by micro-stress, lattice defects, and so on, within the crystallites. For qualitative comparison, however, the equation (28) was used without any change in the calculation of the crystallites sizes.

5. Orientation of crystallites in polycrystalline materials

5-1. Crystallite orientation obtained from x-ray photographic technique

The evaluation of crystallite orientation by x-ray photographic technique has been widely applied in the study of orientation analysis of crystallites because of its easier operation in experiments (Preston 1952, Wardrop 1954, Nitta *et al.* 1973). This technique is based upon the flat-film technique (forward-reflection method), and x-ray beam is irradiated perpendicular to sample surface. As is shown above, this technique gives us only the orientation distribution of lattice planes in crystallites whose poles are exactly on the reflection circle, but can not give us the whole orientation features of crystallites for samples. Besides, this technique have unavoidable drawbacks, which are stemmed from the diffraction geometry, to evaluate three dimensional orientation. They are described in the following (Takahara *et al.* 1965).

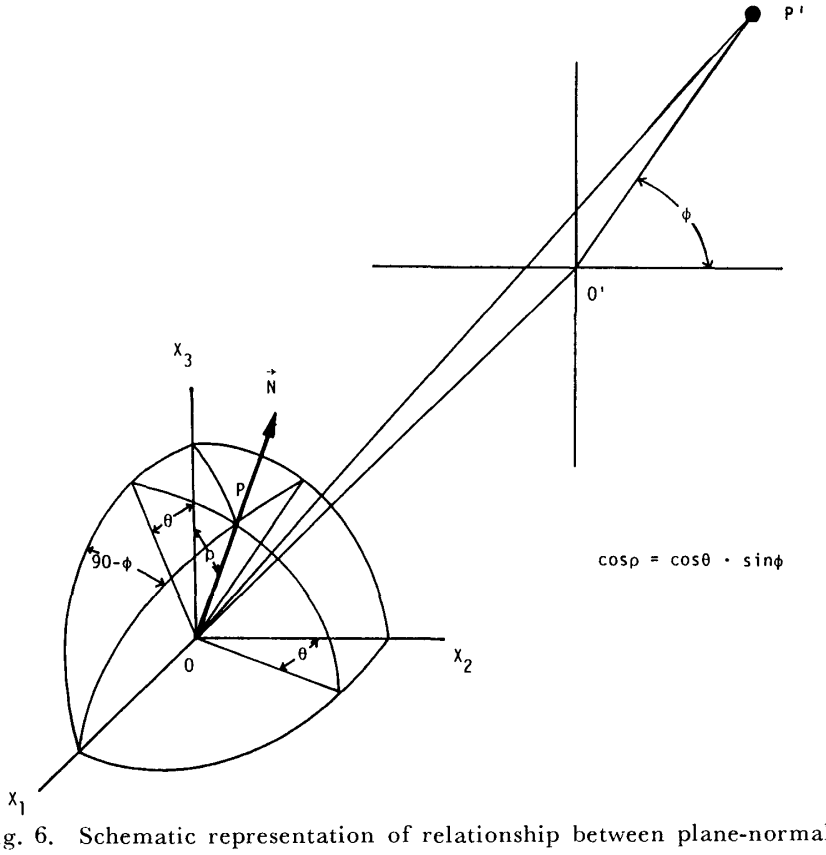

Fig. 6. Schematic representation of relationship between plane-normal and x-ray fiber diagram.

A spherical triangle $\boldsymbol{PX}_1\boldsymbol{X}_3$ is to be considered in Fig. 6. The equation (29) is held between the angles ρ, θ and ϕ,

$$\cos\rho = \cos\theta\cos\phi \tag{29}$$

where ρ is the angle between reciprocal vector $\boldsymbol{h}_{hkl}$ and the axis $\boldsymbol{X}_3$, θ is Bragg angle, and ϕ is the angle between the projection of reciprocal vector $\boldsymbol{h}_{hkl}$ on flat film ($\boldsymbol{OP}'$) and equatorial line. When the angle ϕ ranges from 0 to $\pi/2$, the range of the angle ρ is limited in the range $\theta \leqq \rho \leqq \pi/2$, because the angle ρ changes its value with the change of the value for the angle ϕ. Thus, the reciprocal vector $\boldsymbol{h}_{hkl}$, whose ρ value is in the range from 0 to θ, can not be projected on the flat film, and naturally it is not recorded.

5-2. Crystallite orientations observed from x-ray diffractometer

The flat film method can give all orientation distributions on the reflection circle simultaneously, although the resulting orientation distributions are only a part of the total orientation. The diffractometer technique, however, can give us only a relative orientation distribution value for one position on the reflection circle. The relative orientation distribution value on great circle of Ewald's sphere, however, can be obtained fairly precisely with this technique from the reason discussed above.

The measurement that the scattering of the reciprocal vector $\boldsymbol{h}_{hkl}$, whose top is at the point $\boldsymbol{H}$ and is observed at the point $\boldsymbol{P}$, is considered in Fig. 7. In this case, the line $\boldsymbol{OH}$ is the bisector for the angle $\boldsymbol{BOP}$. Now, if one of the reference axes of sample is set in the perpendicular bisectional plane of the angle $\boldsymbol{BOP}$ which contains the reciprocal vector $\boldsymbol{OH}$ and the sample is rotated around the point $\boldsymbol{O}$ keeping the reference axis in the bisectional plane, only the points on the great circle $\boldsymbol{HH}'$ are able to pass the point $\boldsymbol{H}$ as the sample rotates. Thus, one can obtain the distribution of poles for reciprocal vectors $\boldsymbol{h}_{hkl}$ whose tops are on the great circle of reflection sphere. The orientation distribution of reciprocal vector $\boldsymbol{h}_{hkl}$ in the bisectional

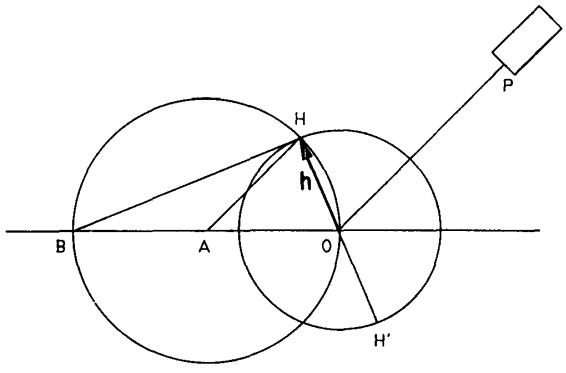

Fig. 7. Geometrical representation of certain reciprocal vector for which x-ray diffraction can be observed at point $\boldsymbol{P}$.

plane can be measured as the scattering intensities by setting a counter on the point ***P***. With the application of this technique, the total orientation distributions of crystallites can be obtained for the sample whose orientation distributions are uniaxial around the reference axis. In general, however, this technique gives only a part of orientation distributions for crystallites in the sample, and the samples should be further rotated around the goniometer axis, in order that all poles for crystallites on the reflection sphere around the point ***O*** can pass the point ***H***.

5-3. Pole figure analysis

The pole figure method was devised so as to obtain the whole orientation features of crystallites in sample space. This method has been widely applied in the studies of metal textures. Recently, this technique has become useful for the orientation studies of polymers (Alexander 1969).

The direction of a plane is described by a relative inclination against the reference plane. The direction is also defined by the inclination of the reciprocal vector or planenormal. The distribution of the plane direction is shown as a set of reciprocal vectors or plane-normals which point out radially from an arbitrary point

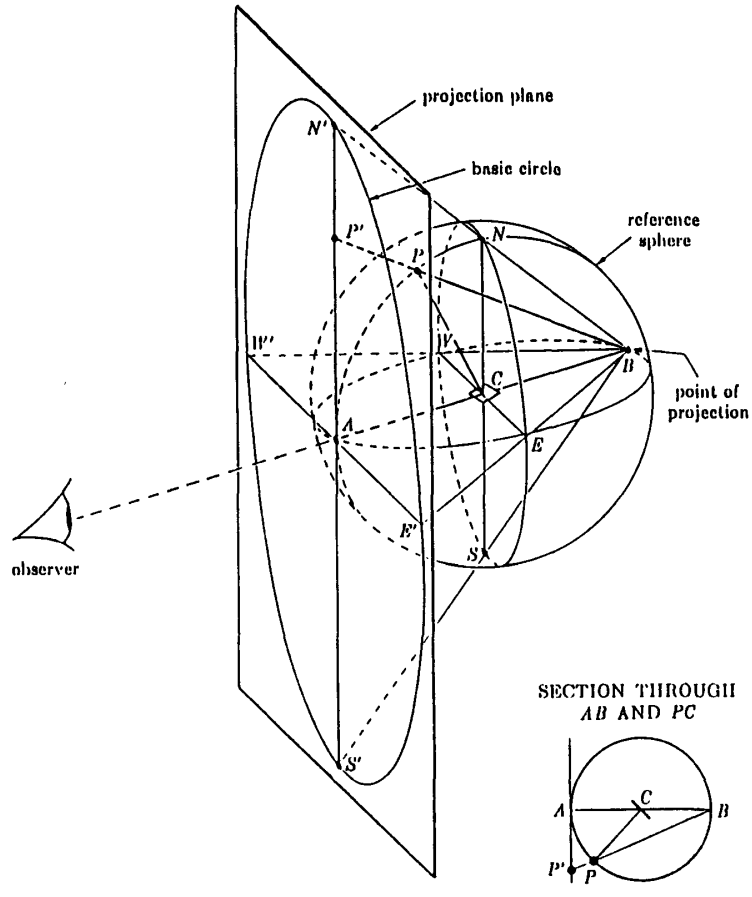

Fig. 3. Stereographic projection.

in a crystal. When this point is set on the center of the reflection sphere, the set of vectors or plane normals are described by a set of their intersecting points on the reflection sphere. These intersecting points are called poles. The positions of poles on the reflection sphere are correspond with the orientational directions of lattice planes, and the density of poles shows the orientation distribution density of the lattice planes. The orientation distributions can be described as the distribution of the poles, when the positions and density distributions of the poles are measured precisely and are described on a two-dimensional map keeping the relations among their positions. The equiangluar stereographic projections, usually used in geography, are suitable for this purpose (Fig. 8, Cullity 1956), and the projection map obtained in this manner is called "pole-figure diagram".

Now, the measurement procedure for the distribution densities of poles to the (*hkl*)-planes on the reference sphere is considered. Two measurement techniques are necessary for these process: one is the transmission technique (Schulz 1949a), and the other is the reflection technique (Schulz 1949b). The outline of these techniques are described as follows.

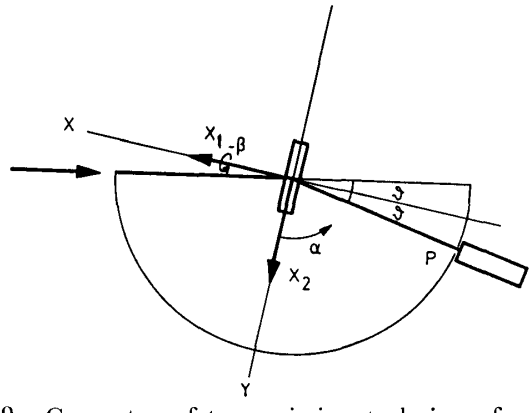

Fig. 9. Geometry of transmission technique for pole figure measurements.

The schematic representation of the transmission technique devised by Schulz is shown in Fig. 9. One of the reference axis for sample is set on the diffractometer axis. The sample geometry at the position for symmetrical transmission technique is selected as a reference geometry, and specified as the sample geometry of $\alpha=0°$ and $\beta=90°$, where the angle α corresponds to the rotational angle for the sample around the diffractometer axis, and the angle β to that around the normal to the sample surface. The orientation distributions for (*hkl*) planes are obtained, when the counter is set in the scattering direction for (*hkl*) planes and the scattering intensities for these planes are observed for various combinations of α and β angles of the sample geometry. The position of poles on the equiagular sterographic projec-

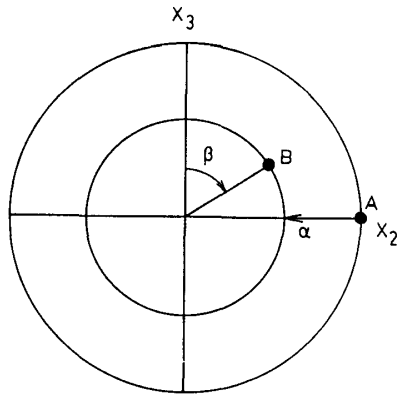

Fig. 10. Schematic representation of location of a pole ($\alpha=0°$, $\beta=90°$).

tion corresponding to the sample geometry $\alpha=0°$ and $\beta=90°$ is located at the point ***A*** in Fig. 10.

It is clear from Fig. 9 that, in the transmission technique, the x-ray beam is interrupted by the frame of sample holder at the sample geometry corresponding to the central area in Fig. 10. For this sample geometry, the reflection technique is suitable for the measurements. Figure 11 shows a schematic representation of the reflection technique. To standardize the representation of the sample geomerty in the reflection technique with that in the transmission technique, the notation for the rotational angles, α and β, is defined as follows. The rotational angle around the normal for the sample surface is defined as β, and that around the horizontal axis perpendicular to the normal for the sample surface is defined as α. The sample geometry is defined as $\alpha=90°$ and $\beta=0°$, when the reference axis fixed on the diffractometer axis in the transmission technique is on this axis. And the scattering intensities for (*hkl*) planes are measured with a counter fixed in the scattering direction for (*hkl*) diffractions at every sample geometry.

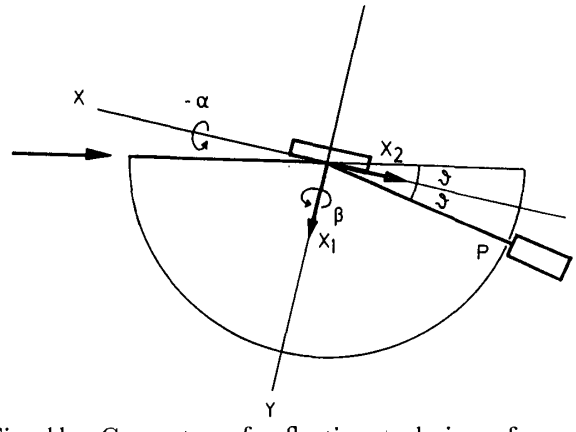

Fig. 11. Geometry of reflection technique for pole figure measurements.

The transmission technique is generally applied in the range from $\alpha=0°$ to $\alpha=60°$, and the reflection technique in the range from $\alpha=40°$ to $\alpha=90°$. The intensities at the sample geometry in the overlapped region of the measurement from $\alpha=40°$ to $\alpha=60°$ were used to calculate the scaling factors which correct the differences in observed diffraction intensities caused by difference of measurement conditions. The total diffraction intensity distributions are, then, obtained.

The three-dimensional diffraction intensity distributions for (*hkl*) planes obtained by above procedure correspond with the density distributions of poles for (*hkl*) planes on the reference sphere. And the pole figure diagram for (*hkl*) plane is obtained, when the pole density distributions calculated from these three-dimensional diffraction intensities for (*hkl*) planes are plotted on the equiangular stereographic projection map.

The pole figure method described here is a general case. This method is applicable only for the materials whose background scattering is very small. This technique should be suitably modified in order to make fully applicable to the measurements of orientation distributions of polymer crystallites whose background scattering is generally large. If the three-dimensional diffraction intensity distributions $I_{hkl}(\alpha, \beta)$ for (*hkl*) planes can be obtained, the three-dimensional orientation distributions for (*hkl*) planes are estimated using the Eq. (31) which was derived by Takahara (1969),

$$N_{hkl}(\phi, \psi)d\psi = KI_{hkl}(\alpha, \beta)d\beta \qquad (31)$$

where the angles ϕ and ψ are the polar and azimuthal angles against the reference axis (Fig. 12).

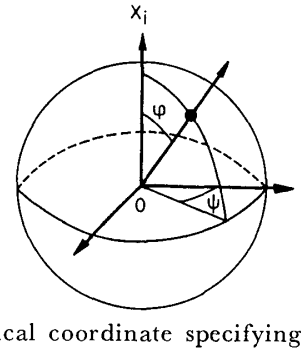

Fig. 12. Spherical coordinate specifying polar angle ϕ and azimuthal angle ψ of a plane-normal with respect to a reference axis $\boldsymbol{X}_i$.

6. Evaluation of orientation for polycrystalline materials

6-1. Representation of average orientation distributions of (*hkl*) planes

The three-dimensional orientation features of (*hkl*)-planes can be represented

diagrammatically on the pole figure diagram. However, by using the average squared cosines of both polar and azimuthal agnles for orientation functions the averaged orientational features of the planes are conveniently and quantitatively expressed. The reference sphere is considered in the sample space (Fig. 12). The pole density distribution functions for (*hkl*)-planes on this sphere are described as $N(\phi, \psi)$. The number of poles (dN) for (*hkl*)-planes in the minute area (dA) on the sphere within the solid angle, $d\phi d\psi$, is given by the Eq. (32).

$$\begin{aligned} dN &= N(\phi, \psi)\, dA \\ &= N(\phi, \psi) \sin\phi d\phi d\psi \end{aligned} \tag{32}$$

The total number of poles (N) for (*hkl*)-planes on the reference sphere is obtained by integrating the both side of the Eq. (32) for whole sphere, and it is represented by the Eq. (33).

$$N = \int_0^{\pi}\int_0^{2\pi} N(\phi, \psi)\, \sin\phi d\psi d\phi \tag{33}$$

Considering the sum of squared directional cosine of the polar angle ϕ, the total sum for all poles on the sphere is calculated with the Eq. (34).

$$\begin{aligned} \Sigma(\cos^2\phi) &= \sum_{\phi}\sum_{\psi} N(\phi, \psi)\cos^2\phi \sin\phi \\ &= \int_0^{\pi}\int_0^{2\pi} N(\phi, \psi)\, \cos^2\phi \sin\phi d\psi d\phi \end{aligned} \tag{34}$$

The average squared directional cosine of polar angle ϕ is described by the Eq. (35).

$$\begin{aligned} \langle\cos^2\phi\rangle &= \frac{\Sigma(\cos^2\phi)}{N} \\ &= \frac{\int_0^{\pi}\int_0^{2\pi} N(\phi, \psi)\, \cos^2\phi \sin\phi d\psi d\phi}{\int_0^{\pi}\int_0^{2\pi} N(\phi, \psi)\, \sin\phi d\psi d\phi} \end{aligned} \tag{35}$$

Similarly the average squared directional cosine for azimuthal angle ψ is obtained with the Eq. (36).

$$\langle\cos^2\psi\rangle = \frac{\int_0^{\pi}\int_0^{2\pi} N(\phi, \psi)\, \cos^2\psi \sin\phi d\psi d\phi}{\int_0^{\pi}\int_0^{2\pi} N(\phi, \psi)\, \sin\phi d\psi d\phi} \tag{36}$$

And the average orientation features can be evaluated by a set of these average squared cosines $\langle\cos^2\phi\rangle$ and $\langle\cos^2\psi\rangle$.

6-2. Representation of average orientation features of crystallites

If the scattering from lattice planes whose reciprocal vectors conicide with the crystallographic axes is nil or very weak, it is generally impossible to evaluate the orientation feature of crystallites. However, Wilchinsky (1959) proposed a general method to give us the average orientation features for any directions in crystallites. The Cartesian coordinate system ***O-xyz*** is fixed on the crystallites (Fig. 13). The

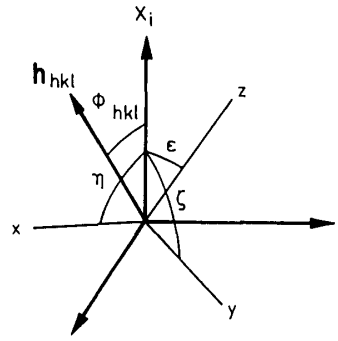

Fig. 13. Coordinate system used for describing a general uniaxial orientation, angular relationship between coordinate system and reciprocal lattice vector $\boldsymbol{h}_{hkl}$.

angles among the coordinate axes (x, y, and z) and the refernce axis (X_i) are described as η, ζ, and ε. Suppose one of the three crystallographic axes is fixed on the z-axis and the other two are unfixed. Then, the reciprocal vector $\boldsymbol{h}_{hkl}$ for lattice plane (hkl) is expanded with unit vectors on the coordinate axes x, y, and z, and the equation (37) is obtained.

$$\boldsymbol{h}_{hkl}=e_{hkl}\boldsymbol{i}+f_{hkl}\boldsymbol{j}+g_{hkl}\boldsymbol{k} \tag{37}$$

where e_{hkl}, f_{hkl}, and g_{hkl} are directional cosine of reciprocal vector $\boldsymbol{h}_{hkl}$ on the coordinate axes x, y, and z. The unit vector on the reference axis X_i is $\boldsymbol{x}_i$, the angle between the vectors $\boldsymbol{h}_{hkl}$ and $\boldsymbol{x}_i$ is $\boldsymbol{\Phi}_{hkl}$, and the equations (38) and (39) are obtained.

$$\boldsymbol{x}_i=(\cos\eta)\boldsymbol{i}+(\cos\zeta)\boldsymbol{j}+(\cos\varepsilon)\boldsymbol{k} \tag{38}$$

$$\begin{aligned}\cos\boldsymbol{\Phi}_{hkl}&=\boldsymbol{h}_{hkl}\boldsymbol{x}_i\\&=e_{hkl}\cos\eta+f_{hkl}\cos\zeta+g_{hkl}\cos\varepsilon\end{aligned} \tag{39}$$

The both side of the Eq. (39) is squared, and averaged for the whole sphere, and the equation (40) is obtained.

$$\begin{aligned}\langle\cos^2\boldsymbol{\Phi}_{hkl}\rangle=&e^2_{hkl}\langle\cos^2\eta\rangle+f^2_{hkl}\langle\cos^2\zeta\rangle+g^2_{hkl}\langle\cos^2\varepsilon\rangle\\&+2e_{hkl}f_{hkl}\langle(\cos\eta)(\cos\zeta)\rangle\\&+2f_{hkl}g_{hkl}\langle(\cos\zeta)(\cos\varepsilon)\rangle\\&+2g_{hkl}e_{hkl}\langle(\cos\varepsilon)(\cos\eta)\rangle\end{aligned} \tag{40}$$

The average squared directional cosine $\langle\cos^2\boldsymbol{\Phi}_{hkl}\rangle$ for the reciprocal vectors $\boldsymbol{h}_{hkl}$ against the reference axis X_i is calculated from the orientation function. The directional cosines e_{hkl}, f_{hkl} and g_{hkl} for the reciprocal vector $\boldsymbol{h}_{hkl}$ on the coordinate axes x, y and z are calculated from lattice constants of the crystal. Then there are six unknown variables in the Eq. (40). If the average squared directional cosines for three crystallographic axes against the reference axis are calculated, a set of six kind of $(\cos^2\boldsymbol{\Phi}_{hkl})$ values can be obtained.

However, from the following trigonometry of the Cartesian coordinate system held among η, ζ, and ε angles (Eq. 41),

$$\langle\cos^2\eta\rangle+\langle\cos^2\zeta\rangle+\langle\cos^2\varepsilon\rangle=1 \quad (41)$$

It is sufficient if a set of five kind of $\langle\cos^2\Phi_{hkl}\rangle$ are calculated. When one applies this procedure to polymers, the number in a set of $\langle\cos^2\Phi_{hkl}\rangle$ becomes even smaller by the selection of Cartesian coordinate system on the crystallites, by the symmetry of the crystallites, and by the combination of lattice planes which are going to be measured.

CRYSTALLITES ORIENTATION OF *Valonia* CELLULOSE AS A MODEL SPECIMEN

1. Introduction

It is well established that cellulose microfibrils are relatively flat ribbons, and that the flatter faces lie parallel to the surface of the cell walls in which they occur (Preston 1951). Since, moreover, in the walls as a whole, the (101) planes of cellulose in the Meyer-Misch unit cell [these planes are indexed as $(2\bar{2}0)$ here, in keeping with the nomenclature presently in use in polymer crystallography] also lie more or less parallel to wall surface, these planes must lie within the microfibril parallel to its flat faces. In cellulosic algae, this uniplanar orientation has been proved by x-ray diffraction for *Valonia* (Sponsler 1931, Preston *et al.* 1937, Frey-Wyssling *et al.* 1951, Schurz 1955, Honjo *et al.* 1958), *Cladophoracae* (Nicolai *et al.* 1938, Astbury *et al.* 1940, Frey-Wyssling *et al.* 1951), green algae (Kreger 1957, Frei *et al.* 1961, Nieduszynski *et al.* 1970), brown algae (Nicolai *et al.* 1938, Astbury *et al.* 1940, Frey-Wyssling *et al.* 1951, Schurz 1955, Kreger 1957, Frei *et al.* 1961, Nieduszynski *et al.* 1970, Preston 1974), red algae (Preston 1974). This is also the case in animal (Schurz 1955) and bacterial (Sisson 1936, Frey-Wyssling *et al.* 1951, Takai *et al.* 1975) cellulose. Even in ramie and cotton fibers (Mukherjee *et al.* 1953), the microfibrillar particles formed by degradation with sulfuric acid tend to lie with this lattice planes along their largest faces. Similar results were obtained for regenerated cellulose both in mercerized fibers (Takahara *et al.* 1968) and sheets (Horio *et al.* 1947, Horio 1950, Takahashi 1969, Matsuo *et al.* 1973, Takai *et al.* 1974). Therefore, the orientation parallel to this lattice plane, the most hydrophilic plane, is regarded as a universal phenomenon in cellulose microfibrils although Okano (1972) found no evidence for uniplanar orientation with *Pinus densiflora* Sieb et Zucc.

The purpose of the investigation described here is an overall estimation of uniplanar orientation in *Valonia* cellulose by means of the x-ray pole figure technique; first, to evaluate the three-dimensional orientation distribution of main crystallographic planes and, secondly, to determine the directions of the molecular and crystallographic axes.

For this purpose I modified the pole figure technique so as to be applicable to

natural cellulose. The validity of the modification of this technique was also discussed.

2. Method of Measurement

X-ray diffractometry is a better tool than birefringence or dichroism to evaluate crystallite orientation simply because the technique responds exclusively to crystallites. The x-ray fiber diagram with the incident beam perpendicular to the fiber axis gives some information regarding the preferred orientation, but when the mode of the preferred orientation is more complex than simple axial, as in *Valonia* cellulose, the intensities of certain reflections have to be estimated both on the inclination angle and on the azimuth of the specimen in order to fully elucidate the orientation that prevails in a specimen. Therefore, the x-ray ploe figure method, which has been widely applied in texture investigation of metal (Cullity 1956), was used throughout the present investigation.

The average degree of biaxial orientation with respect to a reference direction X_i is evaluated in terms of the orientations of the plane normal or reciprocal vector $\boldsymbol{U}_j$ to crystal planes j, expressed as $\langle\cos^2\Phi_{ij}\rangle$ and $\langle\cos^2\Psi_{ij}\rangle$ with $\boldsymbol{U}_j$ specified by Φ_{ij} and Ψ_{ij} in a spherical coordinate system in the sample (Fig. 14 (a)).

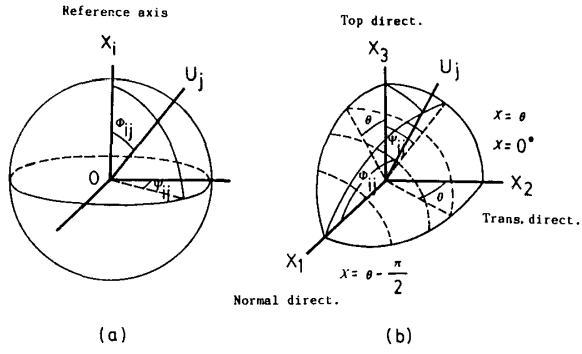

Fig. 14. Spherical coordinates specifying polar angle Φ_{ij} and azimuthal angle Ψ_{ij} of a reciprocal lattice vector with respect to a reference axis $\boldsymbol{X}_i$.

Experimental values of $\langle\cos^2\Phi_{ij}\rangle$ and $\langle\cos^2\Psi_{ij}\rangle$ are determined by averaging $\cos^2\Phi_{ij}$ and $\cos^2\Psi_{ij}$ over an entire surface of the coordinate sphere. However, because of symmetry relationships in the sample, averaging over one quadrant of the sphere is sufficient. These averages are expressed mathematically by two equations (Wilchinsky 1960, Takahara *et al.* 1969).

$$\langle\cos^2\Phi_{ij}\rangle=\frac{\int_0^{\pi}\int_0^{2\pi}N(\Phi_{ij},\Psi_{ij})\cos^2\Phi_{ij}\sin\Phi_{ij}d\Psi_{ij}d\Phi_{ij}}{\int_0^{\pi}\int_0^{2\pi}N(\Phi_{ij},\Psi_{ij})\sin\Phi_{ij}d\Psi_{ij}d\Phi_{ij}} \tag{42}$$

and

$$\langle\cos^2\Psi_{ij}\rangle=\frac{\int_0^{\pi}\int_0^{2\pi}N(\Phi_{ij},\Psi_{ij})\cos^2\Psi_{ij}\sin\Phi_{ij}d\Psi_{ij}d\Phi_{ij}}{\int_0^{\pi}\int_0^{2\pi}N(\Phi_{ij},\Psi_{ij})\sin\Phi_{ij}d\Psi_{ij}d\Phi_{ij}} \tag{43}$$

where $N(\Phi_{ij}, \Psi_{ij})$ is the ple concentration representing the relative amount of crystalline materials having plane normals in the direction given by Φ_{ij}, Ψ_{ij}. The subscripts i and j represent the fact that X_i is taken as a reference axis with respect to the j-th crystal plane of the crystallites.

To be more specific, suppose a spherical corrdinate system $\boldsymbol{O}$-$\boldsymbol{X}_1\boldsymbol{X}_2\boldsymbol{X}_3$ is fixed in a sample, as in Fig. 14 (b), with the X_1 axis normal to the sample surface (thickness direction), the X_2 axis in the transverse direction, and X_3 in the "top" direction, the pole concentration $N(\Phi_{ij}, \Psi_{ij})$ with respect to the X_1 axis at a particular polar angle Φ_{1j} is directly related to the intensity distribution of diffracted x-rays by

$$N(\Phi_{1j}, \Psi_{1j})d\Psi_{1j}=KI_j(\alpha, \beta)d\beta \tag{44}$$

where K is a proportionality constant, $I_j(\alpha, \beta)$ is the azimuthal intensity distribution of x-rays diffracted by the j-th crystal plane. With the reference direction X_1 normal to the sample surface, $I_j(\alpha, \beta)$ is measured by an ordinary horizontal scanning diffractometer, as a function of β while α is held constant at $2\theta_j$, or twice the Bragg angle for diffraction from the j-th crystal plane while keeping the tilt angle of X_1 axis to the incident beam fixed at angle α and rotating the sample around the X_1 axis through the angle β ranging from 0 to π. For determination of $N(\Phi_{1j}, \Psi_{1j})$ as a function of Φ_{1j} as shown in Fig. 14 (b), Ψ_{1j} should range from α to $\theta_j-\pi/2$. Thus, the distribution density $N(\Phi_{1j}, \Psi_{1j})$ with respect to polar angle Φ_{1j} can be obtained for one quadrant of the sphere. This is sufficient for *Valonia* cellulose because of the symmetry of the function.

Furthermore, the average degree of biaxial orientation with respect to another direction, such as the transverse direction X_2 or the top direction X_3, may also be determined in a similar manner from $N(\Phi_{2j}, \Psi_{2j})$ or $N(\Phi_{3j}, \Psi_{3j})$ which can be derived from $N(\Phi_{1j}, \Psi_{1j})$ by re-plotting.

Instead of the above representation in terms of a set of the two quantities, $\langle\cos^2\Phi_{ij}\rangle$ and $\langle\cos^2\Psi_{ij}\rangle$, any two of the three quantities, $\langle\cos^2\Phi_{1j}\rangle$, $\langle\mathrm{con}^2\Phi_{2j}\rangle$, and $\langle\cos^2\Phi_{3j}\rangle$, can be used to express an averaged degree of biaxial orientation, since the following trigonometry is held among these three angles.

$$\langle\cos^2\Phi_{1j}\rangle+\langle\cos^2\Phi_{2j}\rangle+\langle\cos^2\Phi_{3j}\rangle=1 \tag{45}$$

Here, the latter representation is used for biaxial orientation since a graphical representation by Desper's equilateral triangular coordinate system (Desper *et al.* 1966) is easily understood.

Furthermore, Wilchinsky's method (1959), originally developed to determine the

averaged uniaxial orientation for any arbitrary direction within a unit cell, is applied to evaluate the biaxial orientation of the crystallographic axes in the cellulose crystallites. The averaged biaxial orientation can also be evaluated as well when this method is applied for two of the three sample directions along the X_1, X_2, and X_3 axes.

3. Experimental

3-1. Specimen

Two species of *Valonia* were used: *Valonia macrophysa* Kützing and *Valonia forbesii* Harv. These were kindly supplied by Dr. Yasutsugu Yokohama, Marine Biological Laboratory, Tokyo University of Education (Tsukuba University for the present). The specimens were kept in aqueous formaldehyde (formaldehyde/sea water=1/4) with a trace of $CuSO_4$ to prevent any color change. The *Valonia* cell walls were purified by the procedure of Bourret *et al.* (1972). They were washed with 0.1 M-HCI for 6 hr at room temperature and then thoroughly rinsed with twice-distilled water and allowed to dry.

Specimens for pole figure measurements were prepared by parallel stacking of four sheets of *Valonia* cell walls to form a pad approximately 175 μm thick. The parallelism for the stacked cell walls was confirmed by the x-ray flat film camera with every sheet. Specimens for other measurements were single cell walls of *Valonia*.

3-2. Instruments

Two types of x-ray equipments were used in this study. The one was a Shimadzu GX-3B x-ray diffractometer equipped with a Warhus type vacuum camera. This was used for the measurements of x-ray fiber diagrams. Densitometry of the flat film was, then, performed by a Joyce-Loebel double beam recording microdensitometer MK III at the Virus Research Institute, Kyoto University. The other x-ray apparatus was a Rigaku-denki standard type Geigerflex 2011B diffractometer equipped with a manual ploe figure device. This was used for the measurements of three-dimensional orientation distributions of cellulose crystallites.

3-3. Procedure for Ploe-Figure Measurement

Nickel filtered CuKα x-rays generated at 35 kV, 25 mA were employed, and scattering intensities were measured.

The intensities of three main diffraction planes $(2\bar{2}0)$, (220), and (400) on the equator with d=5.96, 5.23, and 3.85 Å were recorded on a strip-chart recorder at 10° intervals over the angular range $0 \leqq \alpha \leqq \pi/2$ and $0 \leqq \beta \leqq \pi$. The intensity data were corrected for air scattering, background noise, the nonrcystalline contribution, and overlap of adjacent diffraction peaks. Corrected intensity data were taken by reflection at α=40°, 50°, 60°, 70°, 80°, 90° and transmission at α=0°, 10°, 20°, 30°, 40°, 50°, 60°, the intensities being measured by both techniques from 40° to 60° permit determination of the scaling factor. Absorption and volume correction factors R for

the transmission technique were calculated using the equation (46) (Cullity 1956):

$$R=\frac{I(\alpha=\alpha)}{I(\alpha=0°)}$$
$$=\frac{\cos\theta[\exp\{-\mu t/\cos(\theta-\alpha)\}-\exp\{-\mu t/\cos(\theta+\alpha)\}]}{\mu t\exp\{-\mu t/\cos\theta\}[\{\cos(\theta-\alpha)/\cos(\theta+\alpha)\}-1]} \quad (46)$$

where μ is the linear absorption coefficient, t is the specimen thickness, θ is the Bragg angle, and α is the latitude. These absorption and volume correction factors were also experimentally evaluated for the reflection technique by using cellulose powder.

4. Results and Discussion

Figure 15 (a) shows a through-view x-ray diffraction pattern of single a *Valonia* cell wall with the x-ray beam perpendicular to the cell wall surface. Two linear arrays of intense arcs at 5.23 Å (220) and 3.85 Å (400) give conculsive proof of the presence of two parallel arrays of cellulose crystallites within the cell wall with crystal axes crossed at somewhat less than 90°, as reported by Preston (1974). However,

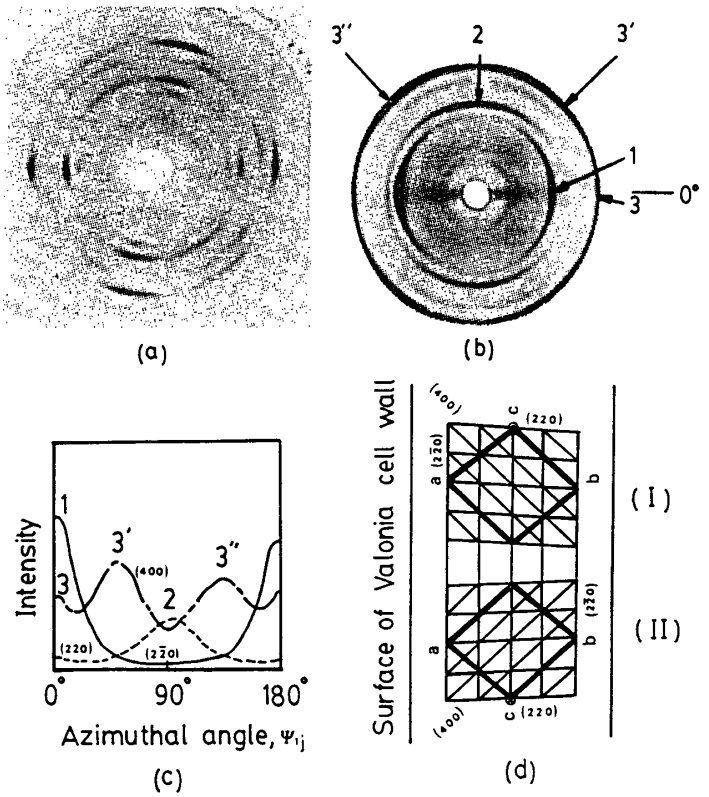

Fig. 15. X-ray diagrams of wall of *Valonia macrophysa* Kützing and the disposition of basal planes: (a) beam normal to wall surface (through-view pattern); (b) beam parallel to wall surface (edge-view pattern); (c) relative values of $I(\Phi, \Psi)$ with respect to azimuthal angle Ψ_{ij} for edge-view pattern starting from the equator, marked 0 in (b). (d) Disposition of the basal planes of the two unit cells necessary to explain (b) and (c).

the arcs at 5.96 Å ($2\bar{2}0$) are clearly present although Preston *et al.* did not detect them. The appearance of ($2\bar{2}0$) arcs in the through-view pattern may be due either to elimination of air scattering by use of the vacuum camera or to imperfect uniplanar orientation of the ($2\bar{2}0$) planes.

An edge-view pattern, with the x-ray beam parallel to the wall surface and along a direction parallel to one of the two sets of microfibrils, and its azimuthal microdensitometer trace [starting from the equator, marked 0 in Fig. 15 (b)] are shown in Figs. 15 (b) and (c). The ars at 5.96 Å (labeled 1) corresponding to ($2\bar{2}0$) planes lying parallel to the c axis (fiber axis), can come from both the transversely and longitudinally oriented microfibrils; while the arcs at 5.23 Å [(220) planes, labeled 2] can come only from the transversely oriented microfibrils. However, the 3.85 Å diffraction [(400) planes] is more complex. The section labeled 3 can come from the longitudinal microfibrils, and 3′ and 3″ from the transverse microfibrils. The two arcs labeled 3′ come from microfibrils within which the disposition of the unit cell is as in Fig. 15 (d) (I). Likewise, the 3″ acrs must be derived from microfibrils with the unit cell as in Fig. 15 (d) (II). Furthermore, on the basis of the unit cell of Fig. 15 (d) (I), the angle between the (220) and (400) plane normals is calculated as 47.1°, which is in good agreement with the observed value.

Figure 16 shows pole figure diagrams for the ($2\bar{2}0$), (220), and (400) planes of cellulose crystallites. These diagrams are drawn on the basis of the stereographic projection along the normal to the cell wall surface. The numerals in the pole figures indicate qualitatively ratios of pole densities. The center of each diagram corresponds to the normal direction of the cell wall surface. In the ($2\bar{2}0$) planes [Fig. 2–3 (a)] the pole density concentrates around the center of the diagram in which the maximum coincides with the center. This suggests that the maximum of the orientation distribution of ($2\bar{2}0$) poles in *Valonia* cell wall is precisely normal to the wall surface. The pole density distribution map is rather elongated in the longitudinal (vertical) direction, which indicates that the ($2\bar{2}0$) pole population is denser along the longitudinal than the transverse direction. In (220) planes [Fig. 16 (b)] all four maxima are on the circumference ($\Phi=90°$) with Ψ angles of 10°, 95°, 190° and 275°. In (400) planes, the pole density maxima are nearly at $\Phi=45°$ with $\Psi=10°$, 95°. 190°, and 275°. The diagram for ($2\bar{2}0$) planes suggests typical uniplanar orientation; and those for (220) and (400) planes two type of uniaxial orientation: i.e., uniplanar-axial in Heffelfinger and Burton's classification (1960). The two mutually crossed sets of pole density maxima are due to the two parallel arrays of cellulose crystallites. Furthermore, it may be shown from the diagrams that there are two mutually antiparallel arrays of "crystallites" in each set of microfibrils. In (220) and (400) diagrams the pole density is greater in the $\Psi=10°$ and 190° regions than in the $\Psi=95°$

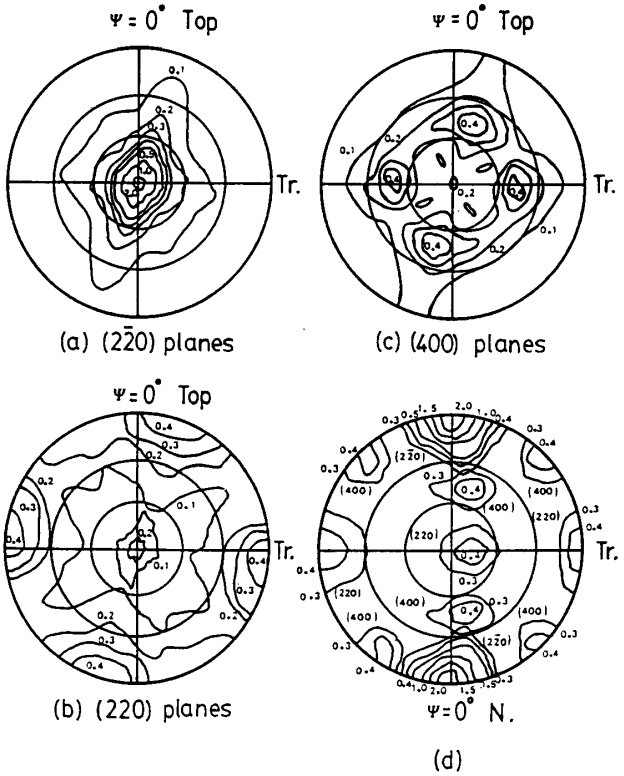

Fig. 16. Projection of hemisphere on $\boldsymbol{X}_2\boldsymbol{X}_3$ plane showing pole distribution for: (a) (2$\bar{2}$0) planes; (b) (220) planes; (c) (400) planes; and (d) projection of hemisphere on $\boldsymbol{X}_1\boldsymbol{X}_2$ plane showing pole distribution for all planes.

and 275° regions. This means that the packing density of cellulose crystallites within the microfibrils is greater in the transverse than in the longitudinal direction. Furthermore, the fact that the pole population is higher along the transverse regions than the longitudinal regions both in (220) and (400) diagrams may reflect the presence of a third minor orientation (Preston 1951). To summarize these pole figure diagrams, the nature of microfibril orientation can be depicted by another pole figure representation in Fig. 16 (d), in which the X_3 direction (top or longitudinal direction) is the axis of the coordinate sphere. In the contour polts, it can be seen that the poles of the (2$\bar{2}$0) planes are rather highly concentrated in the equatorial regions of the coordinate sphere while the (220) and (400) planes are rather widely spread. This representation is consistent with the basal plane model described in Fig. 15 (d).

The degree of biaxial orientation is expressed in terms of $\langle\cos^2\Phi_{1j}\rangle$, $\langle\cos^2\Phi_{2j}\rangle$, and $\langle\cos^2\Phi_{3j}\rangle$. These quantities are used to specify the location of points on the equilateral triangle diagram (Desper *et al.* 1966) as shown in Fig. 17 (a). Only two of three quantities are independent, the third being fixed by equation (45). The location of point (*hkl*) within the $X_1X_2X_3$ triangle depends upon the Miller indices

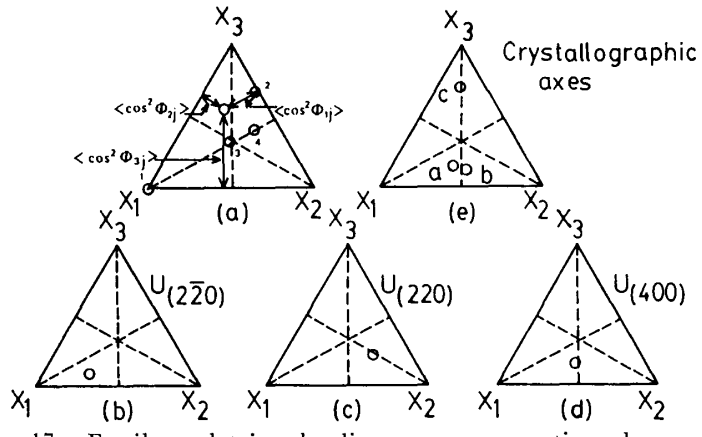

Fig. 17. Equilateral triangle diagrams representing degree of biaxial orientation of the longitudinally aligned *Valonia* cellulose crystallites in terms of three quantities, $\langle\cos^2\Phi_{1j}\rangle$, $\langle\cos^2\Phi_{2j}\rangle$, and $\langle\cos^2\Phi_{3j}\rangle$.

h, k, and l, and the state of orientation of the sample. For example, in Fig. 17 (a), point 1, located at the vertex X_1 would denote perfect orientation parallel to the X_1 axis; point 2, as all other points on side X_2X_3, indicate orientation perpendicular to the X_1 axis. Random orientation of the (*hkl*) normals would result in point 3, with coordinates (1/3, 1/3, 1/3), while uniaxial orientation of the (*hkl*) normals with respect to X_1 would result in a point along the bisector of the angle $X_3X_1X_2$ (for example, point 4).

The degree of biaxial orientation of the (2$\bar{2}$0), (220), and (400) normals within the longitudinally aligned portion of the crystallites in the *Valonia* cell wall are shown in Figs. 17 (b)-(d), respectively. As can be seen in Fig. 17 (b), the (2$\bar{2}$0) normals are almost perpendicular to the X_3 axis (top direction) and preferentially parallel to the X_1 axis (normal direction). In contrast, the location of the (220) plane normals shown in Fig. 17 (c) is characterized by uniaxial orientation around the X_2 axis (transverse direction), while the (400) plane normals [Fig. 17 (d)] exhibit nearly uniaxial orientation around the X_3 axis, intermediate between random and extreme orientation perpendicular to the X_3 axis.

The degree of biaxial orientation of the three principal crystallographic axes within the longitudinally alligned crystallites is expressed in Fig. 17 (e). The ***a*** and ***b*** axes tend to be perpendicular to the X_3 axis, with the ***a*** axis oriented predominantly along X_1 and ***b*** along X_2. On the other hand, the ***c*** axis (fiber axis) naturally tends to lie parallel to X_3. These orientations are in keeping with the orientation model of *Valonia* cellulose crystallites described in Fig. 15 (d). The same argument is valid in the case of transversely alingned crystallites within the *Valonia* cell wall with X_2 and X_3 axes simply exhanged.

5. Summary

From the x-ray pole figure diagrams for *Valonia* cellulose, several facts were found which were described as follows. The $(2\bar{2}0)$ plane normals are almost perpendicular to the sample surface, and the maximum point of the orientation distribution for these plane normals precisely coincided with the normal of sample surface. This means that $(2\bar{2}0)$ crystal planes of *Valonia* cellulose are almost parallel to the cell wall surface, and they have some deviations for their orientations. It is also found that the packing density of cellulose crystallites within the microfibrils is greater in the transverse than in the longitudinal direction. The orientation mode of cellulose crystallites in *Valonia* cell wall has been identified as mutually crossed double uniplanar-axial orientations. The degrees of biaxial orientations for three main crystal planes and three main crystallographic axes have been able to be described quantitatively on the equilateral triangular coordinate systems. From the precise evaluation of the orientation distributions of *Valonia* cellulose, it has, also, been found that there are two mutually antiparallel arrays of cellulose "crystallites" in each orientational set of microfibrils.

CHARACTERIZATION OF CELLULOSE IN COMPRESSION AND OPPOSITE WOOD OF A *Pinus densiflora* TREE

1. Introduction

Structural factors related to mechanical properties of materials are shape and size of molecules, molecular weights, molecular weight distribution, degree of cyrstallintiy, morphology and orientation of crystallites (Nielsen 1975), and their fine structures. The relations between these factors and the mechanical properties of materials have been extensively studied (Ward 1962, Pinnock *et al.* 1966, Nomura *et al.* 1969), but it is hard to report adequate explanations of these relations. The situation is especially unfavorable for wood since this is a complex material which prevents us from reaching meaningful relations between structural factors and mechanical properties. There is, however, a few report which is concerned with a relationship between a mechanical property of wood and its fine structure (Ohgama 1975). The structural factors mentioned above, except the fine structures of wood, was, then, considered in this study.

It is well known that a large variety of characteristics in wood are influenced by the growing conditions, and wood can therefore be used as a suitable material with structural variations. On the other hand, wood is a composite material consisting many different components which renders an explicit analysis difficult. In the present work, I tried to study reaction wood, normal wood and opposite wood, all tissues with different structural features. In woody plants, contrary to herbaceous

plants, it is impossible to effect a bending movement by differential longitudinal grwoth on opposite sides of the organ. Since longitudinal extension growth ceases when secondary xylem being to form, it has therefore been concluded that orientation movements in a stem during secondary growth must involve a bending process, and the stem is exposed to internal stress by expanding or contracting the reaction wood (Wardrop 1964). When the secondary tissues are formed under internal stress, their formation is affected so as to minimize the effect of the stress. Mechanical properties of wood are therefore influenced by the internal stress.

The purpose of the present study was to find a correlation between the mechanical properties of wood and structural factors. Among the structural factors mentioned above, I adopted degree of polymerization, degree of crystallinity, crystalline dimension and crystallite orientation for cellulose as applied to a simplified wood model. And I tried to evaluate these parameters with reaction and opposite wood, and the relations between the values and mechanical properties were discussed.

2. Experimental

2-1. Specimen

A *Pinus densiflora* tree from Kamigamo University Forest, Kyoto University, was studied. It had grown on the top of the mountain and had always been exposed to strong wind. Due to the exposure to wind it contained a large amount of a reaction wood in its stem. Samples were taken from all parts of the stem, and were classified into compression wood and opposite wood.

Wood meal (40–80 mesh) was used for measuring the degree of polymerization and degree of crystallinity of cellulose, while block samples (20×20 mm, thickness: 1 mm) were used for measurements of the cellulose orientation and of crystallite size.

2-2. Degree of Polymerization

Wood meal was delignified according to Klauditz method (1957). It was nitrated by the method of Alexander and Mitchell (1949), and its intrinsic viscosity was determined in n-butyl acetate at 30°C (Goring *et al.* 1960, 1962). No correction for shear dependence was made. Nitrogen contents varied from 12.0% to 14.0%. Since the nitrogen content of cellulose nitrate of a given molecular weight is an important factor influencing solution viscosity (Lindsley *et al.* 1953), all intrinsic viscosity values $[\eta]$ were calculated for the theoretical level of trisubstitution $[\eta]_T$, using the empirical equation derived by Lindsley and Frank (1953):

$$\log\frac{[\eta]_T}{[\eta]} = \log f_x + (14.15 - x) \cdot B \tag{47}$$

where f_x ($=1.833-0.0589x$) is a factor related to the departure of the unit molecular weight from that of cellulose trinitrate, x is percentage of nitrogen content in the

sample, and B is an empirical constant, having a value 0.114 for all the cellulose samples studied. The degree of polymerization was calculated using the following equation (Goring *et al.* 1960, 1962):

$$\log [\eta]_T = 0.5719 \cdot \log DP + 0.5556 \quad (48)$$

2-3. Description of X-ray Equipments

A rotating anode x-ray diffractometer system (Rigaku-denki Rotaflex RU-3L) and a sealed x-ray tube diffractometer system (Rigaku-denki Geigerflex 2011B) were used to evaluate x-ray diffraction intensities. Measurements were carried out with a fiber attachment on the goniometer. Both transmission and reflection techniques were used.

2-4. Degree of Crystallinity

Degree of crystallinity was measured with wood meal by reflection and by continuous scanning techniques using the Rigaku-denki Geigerflex 2011B. The sample was formed into a disk (20 mmϕ, thickness: 1 mm). The scanning ranged from 5° to 30° for 2θ (θ: Bragg angle). The diffraction curves were corrected for air and background scanning. No corrections for irradiated volume were made. The corrected x-ray diffraction patterns were divided into amorphous and crystalline regions by the method developed by Jayme *et al.* (1964). The degree of crystallinity was calculated from the following equation:

$$DC = \frac{I_{cry}(2\theta)\, d(2\theta)}{I_{am}(2\theta)\, d(2\theta) + I_{cry}(2\theta)\, d(2\theta)} \cdot 100 \ (\%) \quad (49)$$

where $I_{am}(2\theta)$ and $I_{cry}(2\theta)$ are intensities for amorphous and crystalline regions, respectively.

2-5. Orientation of Crystallites

For the conventional representation of the orientation of cellulose crystallites in wood, the fibrilar angles of cellulose microfibrils in wood were measured on the assumption that the orientation functions for cellulose crystallites in wood had cylindrical symmetries.

Crystallite orientations were measured with block samples of wood by the symmetrical transmission technique, using the Rigaku-denki Rotaflex RU-3L equipped with a fiber attachment on the goniometer. The sample was rotated around the normal axis of the sample surface and x-ray intensity variations were recorded for (040) planes. This means that the orientation distribution of crystallographic ***c***-axes (fiber axis) of cellulose crystallites in the wood is recorded. No corrections were made for these intensity variations.

2-6. Size of Crystallites

The same block samples for orientation studies were used to measure size of the crystallites. The measurements were made by the transmission technique using

the Rigaku-denki Rotaflex RU-3L with the fiber attachment. The samples were rotated around their plane normals until (002) and (040) reciprocal vectors were in the horizontal plane, respectively to record x-ray diffraction intensities. The diffraction curves were corrected for air and background scatterings, and the crystalline scatterings were separated from the total scatterings. Integral breadth from intensity curves for crystalline regions were corrected for instrumental broadening by the method developed by Jones (1938), using hexamethylenetetramine crystals. With the aid of these corrected integral breadth, size of cellulose crystallites in the wood was calculated along the (002) and (040) directions, using the Scherrer's equation (Eq. 50).

$$D=\frac{0.94\lambda}{\beta_0 \cos\theta} \tag{50}$$

where λ is a wave length of x-ray, β_0; corrected half breadth of line profile, θ; Bragg angle. The step scanning technique and a point focus x-ray optical system were used in these measurements.

3. Results and Discussion

The most of the compression wood occurred was between 1 m and 2.5 m above the ground. Figure 18 shows the degree of polymerization of cellulose in compression and opposite wood at different distance from the ground. Hardly any difference was noticed between compression and opposite wood in *DP* values, but they were somewhat lower in the region where most of the compression and opposite wood occurred. Since *DP* is considered to be affected by tensile stress more than by com-

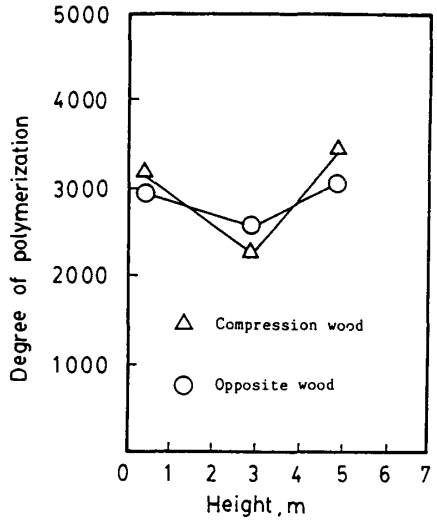

Fig. 18. Degree of polymerization of cellulose in compression and opposite wood of *Pinus densiflora* versus distance above the ground.

pressive stress, it is difficult to understand why *DP* was lower in this region. The polymerization process of glucose to cellulose might somewaht be retarded in this region.

Figure 19 shows the degree of crystallinity of cellulose in compression and opposite wood at different distances from the ground. The value for normal wood is also plotted for comparison. The value for the degree of crystallinity for opposite wood was 50–60%, about 50% for normal wood, and 45–50% for compression wood. The crystallinity decreased with increasing height above the ground.

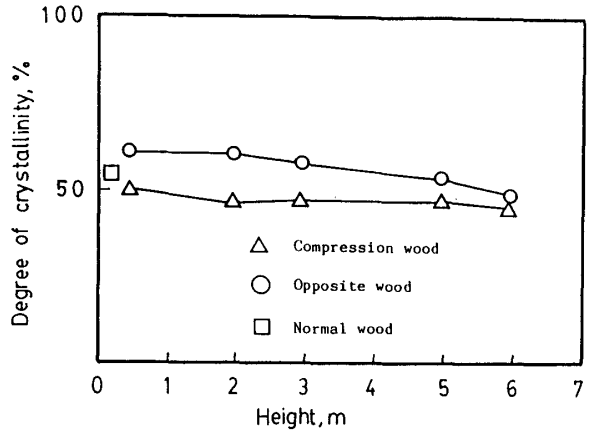

Fig. 19. Degree of crystallinity for cellulose crystallites in *Pinus densiflora*.

It is well recognized that crystalline materials are hard and brittle, and are easily fractured under strong compressive force, whereas, amorphous materials can easily be deformed by converting mechanical energy into thermal energy. As the compressive stress becomes larger, the repulsive force between atoms plays a stress-bearing role, and much energy is required until amorphous materials are completely broken. Materials with a low degree of crystallinity therefore have a higher compressive strength. It has long been known that compression wood has a high compressive and a low tensile strength (Onaka 1949). The fact that cellulose has a lower degree of crystallinity with increasing stem height is probably to be attributed to the magnitude of the strain.

Figure 20 shows the two dimensional orientation distribution of the cellulose crystallites. This is a projection on the plane parallel to the stem axis. The maximum point of **c**-axis orientation distribution for cellulose crystallites in compression wood is at $\phi=30°$, and in opposite wood at $\phi=0°$. The same point in noraml wood is at $\phi=25°$, which is not shown in Fig. 20.

Crystalline materials are hard to defrom under tensile stress, since the energy required for deformation of crystallites is of the order of covalent bond energy, which

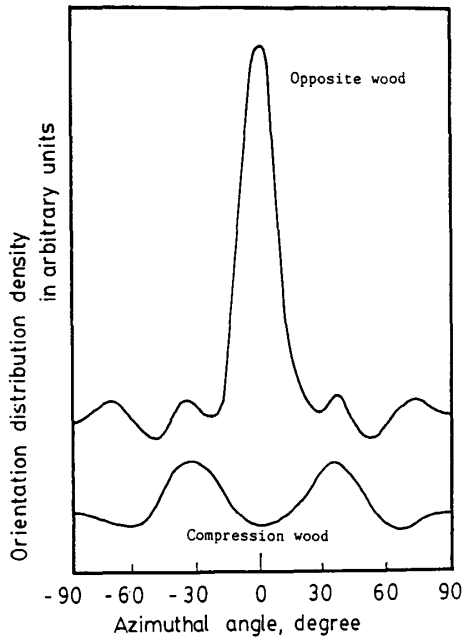

Fig. 20. Orientation distribution of cellulose crystallites in *Pinus densiflora*.

is extremely large, whereas in amorphous materials Van der Waals force or H-bond energy play a load-bearing rloe in the deformation process, and their energy is converted into thermal energy while molecular slippage is taking place. Thus a higher degree of crystallinity and parallel orientation of the cellulose crystallites, should lead to a higher Young's modulus and a higher tensile strength. The tensile breaking strength of normal wood is higher than that of compression wood in agreement with these arguments. Opposite wood has higher tensile breaking stength than normal wood.

Figure 21 shows the cellulose crystallite dimension parallel to the (002) plane direction in compression and opposite wood, plotted against the distance from the ground. The value for opposite wood is 3.5 nm (corresponding to four or five cellulose unit cells), in compression wood, 3.1 nm (corresponding to four cellulose unit cells). The crystallites in opposite wood are one unit cell larger along the [002] direction than in compression wood. The value for normal wood is about 3.2 nm, which in not shown in Fig. 21. However, considering the precision of the measurements and Scherrer's equation, it might be concluded that in wood the cellulose crystallites have essentially the same transverse dimension.

It is a well-established fact that in syntheitc polymer there is a definite relationship between chain orientation and tensile stress: the chains in an amorphous region are oriented as they are stressed, and the degree of orientation is directly related to the magnitude of the tensile stress. The same argument would be valid for the relation-

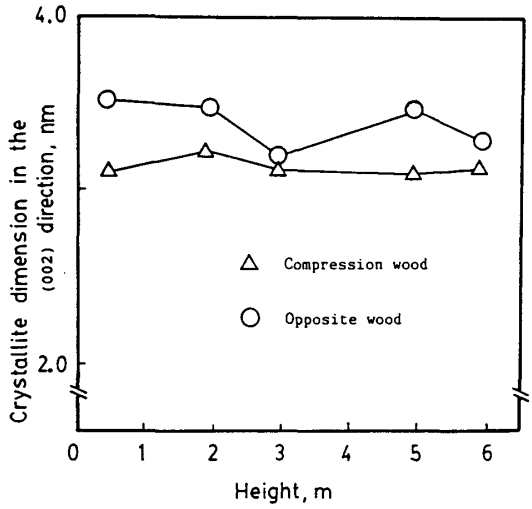

Fig. 21. Crystallite dimension parallel to (002) plane of cellulose crystallites in *Pinus densiflora*.

ship between the chain orientation of cellulose in wood and the internal stress. The degree of orientation should accordingly increase in the order opposite wood>normal wood>compression wood. Furthermore, the lateral order of chains in the region near the crystallites is especially good and almost equal to that of the chains in the crystalline regions. Therefore, it is probable that the cellulose crystallite dimension estimated by the x-ray diffraction method is somewhat larger in opposite wood.

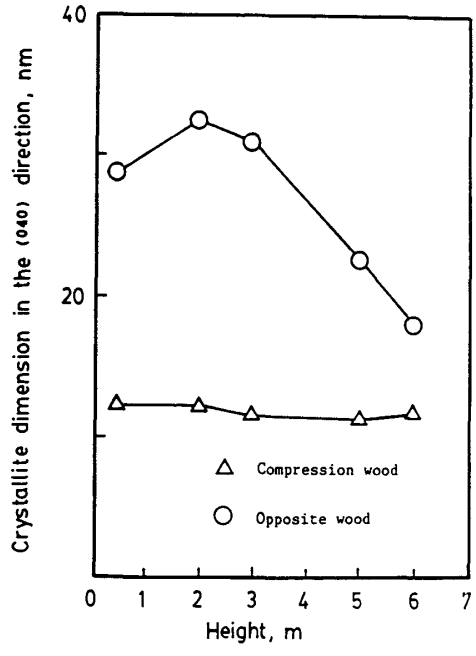

Fig. 22. Crystallite dimension parallel to (040) plane of cellulose crystallites in *Pinus densiflora*.

In Fig. 22 the dimension of the cellulose crystallites parallel to the (040) plane direction, that is the longitudinal direction of the cellulose crystallites, is plotted against the distance from the ground in both compression and opposite wood. The difference between compression and opposite wood is large. In opposite wood, the cellulose crystallite dimension is 17.5–32.5 nm (corresponding to 17–32 cellulose unit cells). In compression wood, it is about 12 nm (corresponding to 11–12 cellulose unit cells). It is believed that in opposite wood, which is under tensile stress, the cellulose chains are arranged in the direction of the tensile stress and the lateral order of the chains is fairly good in the longitudinal direction, and the longer crystallites are formed. In compression wood, which is under compressive stress, on the other hand, the cellulose chains form a random coil and the lateral orderedness of the chains is good only within a short range, and only short crystallites can be formed. As is seen in Fig. 22, cellulose crystallite size in compression wood is independent of the stem height, but apparently a difference exists in opposite wood. In opposite wood, the cellulose crystallites reached their maximum size in the region between 1m and 2.5m above the ground where most of the compression wood occrurred. Accordingly, one can argue that the tensile stress in opposite wood is largest where the compression is most prevalent, and above this regions, the higher the position, the smaller tensile stress is expected to be.

From the above discussion and the hypothesis published by Wardrop (1964) (see Introduction of this section) it is expected that there is a close relation between the morphology of the crystallites in *Pinus densiflora* and the distribution of growth stresses in the tree. The opposite wood under tensile stress has longer cellulose crystallites with a higher degree of crystallinity. It also has a better orientation distribution of the cellulose crystallites in the longitudinal direction. The tensile strength of opposite wood in the longitudinal direction is therefore higher, whereas its compressive strength is lower. The compression wood which is under compressive stress has shorter crystallites with lower degree of crystallintiy, and the angle between the stem and the orientational direction of the cellulose crystallites is large. The compression wood therefore has a high compressive and a low tensile strength. It is expected that normal wood should have a strenght between that of the compression and the opposite wood.

4. Summary

The structural factors in a *Pinus densiflora* tree grown under the influence of strong wind were studied. No *DP* difference for cellulose molecules was noticed between the compression and the opposite wood, but the *DP* was somewhat lower in the region where the compression wood was concentrated. The degree of crystallinity of cel-

lulose was 45–50% in the compression wood, about 50% in the normal wood, and 50–60% in the opposite wood. The crystallinity decreased with increasing height above the ground. The maximum point of crystallographic **c**-axis (fiber axis) orientation distribution for cellulose crystallites in the compression wood located at $\phi=30°$, in the normal wood at $\phi=25°$, and in the opposite wood at $\phi=0°$. The cellulose crystallite dimension in the transverse direction was 3.2 nm, corresponding to four cellulose unit cells, a value that was almost constant throughout the wood. In the longitudinal direction, there was large difference in cellulose crystallite dimension between the compression and the opposite wood. In the compression wood the cellulose crystallite dimension was 12 nm corresponding to 11–12 cellulose unit cells. In the opposite wood it was 17–32.5 nm corresponding to 17–32 cellulose unit cells. These sturctural factors were apparently affected by the environmental conditions, and the mechanical properties of the wood were influenced by these factors. The opposite wood had longer crystallites, a higher degree of crystallinity and a better orientation distribution of cellulose crystallites in the longitudinal direction. The compression wood, on the other hand, had shorter crystallites, a lower degree of crystallinity and a large angle between the stem and the direction of the crystallites.

THREE-DIMENSIONAL ORIENTATION OF CELLULOSE CRYSTALLITES IN WOOD

1. Introduction

The orientation of cellulose crystallites in wood has been studied from structural and physiological points of view, and it was recently found that the orientation distribution of cellulose crystallites plays an important role in the elastic properties of wood, and affects Young's modulus of wood in the longitudinal direction (Norimoto *et al.* 1981). Therefore a quantitative evaluation of the three-dimensional orientation distributions of cellulose crystallites in wood would be useful for characterization of the mechanical properties of wood.

The planar orientation mode of cellulose crystallites in the cell wall, which has first observed by Preston (1951) in *Valonia ventricosa,* has been found in many kinds of lamellated marine algal cell walls. The same modes was also found in bacterial, animal, and regenerated celluloses. The planar orientation mode is a universally observed phenomenon in the orientation distribution of cellulose crystallites. Whether this planar orientation mode also exists in the wood cell wall has been argued by many investigators. Using a cylindrically shaped specimen on the goniometer axis, Okano (1972) measured the intensity distribution of three main paratropic reflections and concluded that no preferred orientation existed in the wood cell walls, because no deviations were detected for the positions of the maximum points in these

reflections. I examined the probability of a cylindrical symmetry for the orientation distribution of cellulose crystallites around the longitudinal axis in the cell walls and found that cellulose crystallites showed a random orientation distributions in the plane perpendicular to this axis, from the study of x-ray diffraction patterns of pressed wood samples (Tanaka *et al.* 1974). This was semi-quantitatively confirmed in *Pinus densiflora* opposite wood (Tanaka *et al.* 1980). These results were recently confirmed by Revol *et al.* (1982) in their x-ray and electron diffraction studies on pressed wood samples. These investigators, however, were confronted by following technical difficulties owing to geometrical heterogeneity of the wood cell wall: (1) the cross sectional shape of pressed wood cell walls is heterogeneous, (2) x-ray or electron beam has a limited cross sectional area and can not be treated as a point. Furthermore, they obtained only a part of orientation distribution of cellulose crystallites in wood, and did not the whole distributions of them. The possibility for a planar orientation, therefore, should not be neglected. The orientation of cellulose crystallites in wood was treated only in an ideal situation by the above investigators because their orientation measurement of cellulose crystallites were only qualitative or at most semi-quantitative.

For a more quantitative and precise study of the orientation distribution of cellulose crystallites, the modified pole figure technique (Tanaka *et al.* 1977) was applied in this study, which was found to be useful for the orientation study of *Valonia* cellulose. When this technique was applied for the opposite wood of *Pinus densiflora,* the orientational feature of (040) planes, which had somewhat sharp orientation distributions, was able to be described, but not for other crystallographic planes (Tanaka *et al.* 1980). The orientational feature for (101) and ($10\bar{1}$) planes, which were mutually overlapped, was especially difficult to be shown. Then, modifying the technique I found that by trial and error the broad line profile for diffraction peak could be approximated by Gaussian. Assuming the diffraction peak as a Gaussian the overlapped (101) and ($10\bar{1}$) peaks were divided by a mathematical procedure based on the least square method. Thus the random error was avoided in the separation of overlapped peaks. The pole figures for (101), ($10\bar{1}$), (002), and (040) planes were mapped by the orientation functions calculated from the diffraction intensity distributions obtained with the above procedure. I also devised an evaluation procedure for the orientation of wood cellulose based on both pole figures of wood cellulose and wood anatomy (Tanaka 1983), and tried to evaluate the three-dimensional orientations of wood cellulose with this procedure, and finally the orientation mechanisms of cellulose crystallites in wood was discussed (Tanaka *et al.* 1984).

2. Fine structure of wood and pole figures of wood cellulose

Wood is considered as an aggregate of the cell walls which are composed of large number of microfibrils as the structural unit, and each microfibrils is consisted of many cellulose crystallites. Therefore, when one speaks of the orientation of wood, one has to consider the orientation of each element, the orientation of cell wall, microfibril, and crystallites, with respect to the initial coordinates.

It is, however, difficult to obtain information on one sheet of cell wall by x-ray diffraction technique from the following technical point of view: (1) x-ray diffraction measurement gives us only averaged information of the whole wood sample and (2) x-ray beam is usually larger than the dimenison of wood cell wall. Thus one can not discuss the structural feature of wood cellulose from the information of x-ray measurements directly, and it is necessary to consider the structural feature of cellulose in every structural element to relate each other. After these procedures the structural feature can be compared with the experimental data. For this purpose, Cartesian coordinate systems are fixed on every structural element, which are linearly translated.

Figure 23 shows the Cartesian coordinate systems fixed on cellulose crystallite, microfibril, cell wall, sample block of wood which are all the structural units of wood. The coordinate system $O\text{-}XYZ$ is fixed on the crystallite. The direction of the reciprocal vector U_j in the cooordinate system can be described by both polar (Θ_j) and azimuthal (Φ_j) angles. In the same manner, $O\text{-}X_1Y_1Z_1$, Θ_j' and Φ_j' are for the coordinate system fixed on the microfibril, $O\text{-}X_2Y_2Z_2$, Θ_j'' and Φ_j'' for the coor-

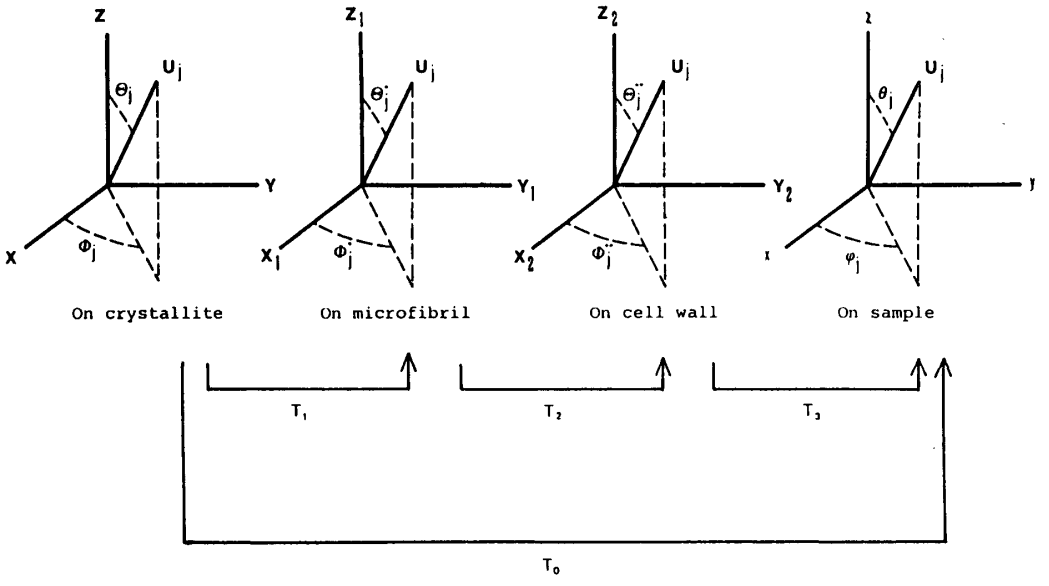

Fig. 23. Cartesian coordinate systems fixed on orientational units in wood and the linear translations between them.

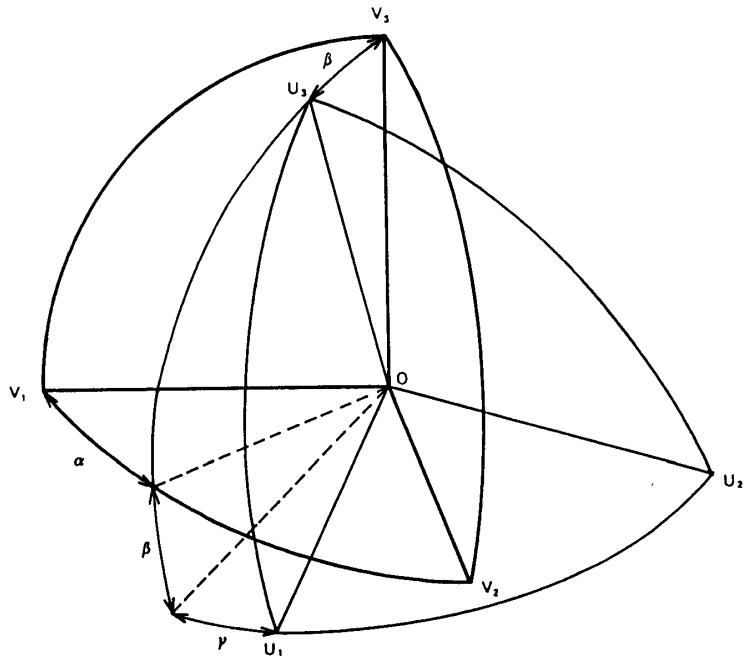

Fig. 24. Relationship between two Cartesian coordinate systems, $\boldsymbol{O}$-$\boldsymbol{U}_1\boldsymbol{U}_2\boldsymbol{U}_3$ and $\boldsymbol{O}$-$\boldsymbol{V}_1\boldsymbol{V}_2\boldsymbol{V}_3$. α, β, and γ are Euler angles.

dinate system fixed on the cell wall, and $\boldsymbol{O}$-$\boldsymbol{xyz}$, θ_j and ϕ_j for the coordinate system fixed on the sample block. The pole figure diagram is then, equivalent to the three dimensional orientation distribution in the coordinate system $\boldsymbol{O}$-$\boldsymbol{xyz}$ for the corresponding reciprocal vectors fixed on the coordinate system $\boldsymbol{O}$-$\boldsymbol{XYZ}$. Three linear translations, $\boldsymbol{T}_1$, $\boldsymbol{T}_2$, and $\boldsymbol{T}_3$, are now considered (Fig. 23), and the linear translation between the coordinate systems, $\boldsymbol{O}$-$\boldsymbol{U}_1\boldsymbol{U}_2\boldsymbol{U}_3$ and $\boldsymbol{O}$-$\boldsymbol{V}_1\boldsymbol{V}_2\boldsymbol{V}_3$, is considered. This translation is shown in Fig. 24. These two coordinate systems are related with three Euler angles, α, β and γ. The unit vectors $\boldsymbol{U}_j$ in both $\boldsymbol{O}$-$\boldsymbol{U}_1\boldsymbol{U}_2\boldsymbol{U}_3$ and $\boldsymbol{O}$-$\boldsymbol{V}_1\boldsymbol{V}_2\boldsymbol{V}_3$ systems are related by Eq. (51).

$$\begin{pmatrix}\sin\theta_j\cos\phi_j\\ \sin\theta_j\sin\phi_j\\ \cos\theta_j\end{pmatrix}=T(\alpha,\beta,\gamma)\begin{pmatrix}\sin\Theta_j\cos\Phi_j\\ \sin\Theta_j\sin\Phi_j\\ \cos\Theta_j\end{pmatrix} \tag{51}$$

where $T(\alpha,\beta,\gamma)$ is the translation matrix given by Eq. (52).

$$T(\alpha,\beta,\gamma)=\begin{pmatrix}\cos\alpha\cos\beta\cos\gamma-\sin\alpha\sin\gamma & -\cos\alpha\cos\beta\sin\gamma-\sin\alpha\cos\gamma & \cos\alpha\sin\beta\\ \sin\alpha\cos\beta\cos\gamma+\cos\alpha\sin\gamma & -\sin\alpha\cos\beta\sin\gamma+\cos\alpha\cos\gamma & \sin\alpha\sin\beta\\ -\sin\beta\cos\gamma & \sin\beta\sin\gamma & \cos\beta\end{pmatrix} \tag{52}$$

The linear translations are defined among the Cartesian coordinate systems fixed every structural unit as given by Eq. (53).

$$\begin{aligned}
&[\boldsymbol{O}\text{-}\boldsymbol{XYZ}] \xrightarrow[T_1(\alpha_1, \beta_1, \gamma_1)]{} [\boldsymbol{O}\text{-}\boldsymbol{X_1Y_1Z_1}] \\
&[\boldsymbol{O}\text{-}\boldsymbol{X_1Y_1Z_1}] \xrightarrow[T_2(\alpha_2, \beta_2, \gamma_2)]{} [\boldsymbol{O}\text{-}\boldsymbol{X_2Y_2Z_2}] \\
&[\boldsymbol{O}\text{-}\boldsymbol{X_2Y_2Z_2}] \xrightarrow[T_3(\alpha_3, \beta_3, \gamma_3)]{} [\boldsymbol{O}\text{-}\boldsymbol{xyz}]
\end{aligned} \tag{53}$$

The linear translation (Eq. 54) is, further, defined between the reciprocal vector in a crystallite and the same vector in a sample space, namely, between the coordinate system $\boldsymbol{O}\text{-}\boldsymbol{XYZ}$ and $\boldsymbol{O}\text{-}\boldsymbol{xyz}$.

$$[\boldsymbol{O}\text{-}\boldsymbol{XYZ}] \xrightarrow[T_0(\alpha_0, \beta_0, \gamma_0)]{} [\boldsymbol{O}\text{-}\boldsymbol{xyz}] \tag{54}$$

The equation (54) can be derived as the combination of three translations (Eq. 53), which is given by Eq. (55).

$$\boldsymbol{T}_0(\alpha_0, \beta_0, \gamma_0) = \boldsymbol{T}_3(\alpha_3, \beta_3, \gamma_3)\boldsymbol{T}_2(\alpha_2, \beta_2, \gamma_2)\boldsymbol{T}_1(\alpha_1, \beta_1, \gamma_1) \tag{55}$$

In coordinate system $\boldsymbol{O}\text{-}\boldsymbol{XYZ}$, the X-axis conicides with crystallographic a-axis, and Y-axis with b-axis. Similarly, in coordinate system $\boldsymbol{O}\text{-}\boldsymbol{X_1Y_1Z_1}$, Z_1-axis coincides with the microfibril axis, X_1-axis with an axis perpendicular to the microfibril axis, and in coordinate system $\boldsymbol{O}\text{-}\boldsymbol{X_2Y_2Z_2}$, X_2-axis coincides with the normal to cell wall surface, Z_2-axis with the longitudinal axis of wood cells, and in coordinate system $\boldsymbol{O}\text{-}\boldsymbol{xyz}$, $\boldsymbol{x}$-axis coincides with radial axis of wood, $\boldsymbol{z}$-axis with longitudinal axis of wood. Then, α_1, β_1, α_2, β_2, β_3, and γ_3 become fixed parameters, and γ_1, γ_2, and α_3 are variable parameters. Only have to solve these three variable parameters have to be solved.

Based on the above geometry, two kinds of pole figure diagrams are considered in the case of both axial and planar orientation modes. First, in the case of the axial orientation mode of cell wall in which the cellulose crystallites are oriented uni-axially within the cell wall, the whole wood also shows a uni-axial orientation mode around the longitudinal reference axis. In this case, the pole figure diagrams of cellulose crystallites in the wood cell wall (for the croodinate system $\boldsymbol{O}\text{-}\boldsymbol{X_2Y_2Z_2}$) are as shown in Fig. 25 (a)-(d). If the orientation distribution functions of cellulose crystallites is independent of at least one of two variables, γ_1 and γ_2, the same pole figure diagrams are obtained for three paratropic reflections, (101), ($10\bar{1}$), and (002) planes as shown in Fig. 25, (a)-(c). And if the orientation distribution function is independent of the variable α_3 only, a cylindrical symmetry around the longitudinal direction results, and the same pole figure diagrams for wood sample are obtained for three paratropic reflections, i.e. (101), ($10\bar{1}$) and (002) planes, as shown in Fig. 25, (e)-(g). The cross-sectional shape of wood cell wall is nearly rectangular, and actually α_3 dependence of orientation functions is present. When the orientation depends only on α_3 the paratropic reflections, i.e. (101), ($10\bar{1}$) and (002) planes, show exactly the same orientation distribution patterns.

Secondly in the case of planar orientation mode of cell wall in which the cellulose

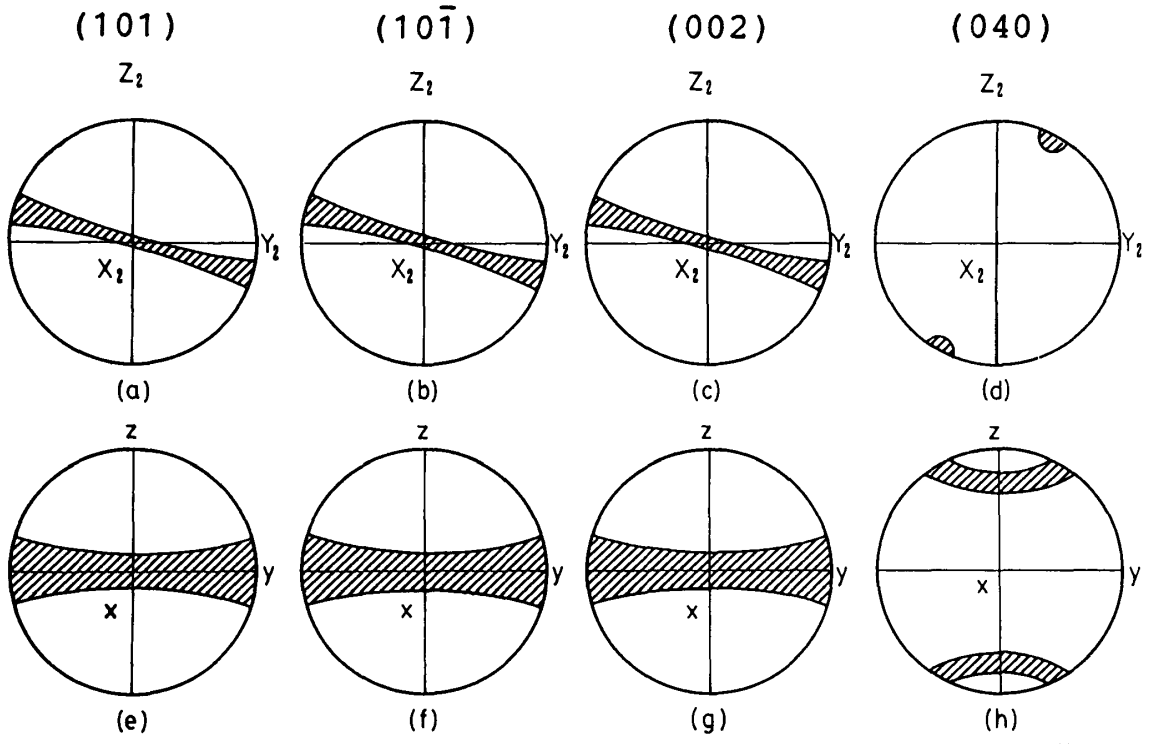

Fig. 25. Ideal pole density distributions of cellulose crystallites in wood and cell walls in the case of axial orientation.

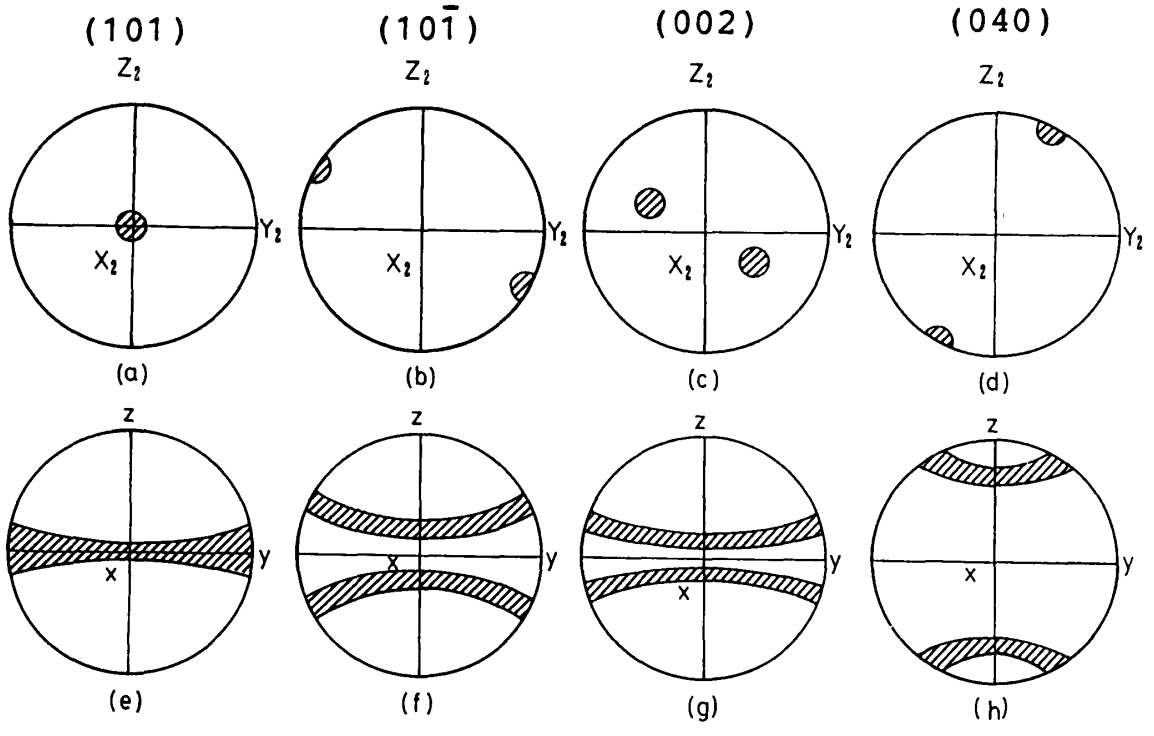

Fig. 26. Ideal pole density distributions of cellulose crystallites in wood and cell walls in the case of planar orientation.

crystallites are parallel to the lumen of the cell wall, and ***c***-axis of crystallites is parallel to certain axis of the cell wall. In actual wood the planar orientation of cellulose crystallite means a uniplanar-axial orientation with respect to cell wall and uni-axial orientation with respect to the whole wood. Thus the orientation mode in wood is complex and quite different from synthetic polymers in which the planar orientation is prevalent. In wood the orientation functions are dependent both on γ_1 and γ_2 values, and have distributions only at special γ_1 and γ_2 values. Therefore, α_1, β_1, γ_1, α_2, β_2, γ_2, β_3, and γ_3 become the fixed parameters and only α_3 remains as a variable. Figure 26 (a)-(d) show these orientation features in cell wall (in coordinate system $\boldsymbol{O}$-$\boldsymbol{X}_2\boldsymbol{Y}_2\boldsymbol{Z}_2$). In these diagram, three paratropic reflections, i.e. (101), (10$\bar{1}$), and (002), are different each other [Fig. 26 (a)-(c)], and are quite different from the case of axial orientation. And if the orientation functions of cellulose crystallites have no dependence upon the variable α_3, the pole figure diagrams for whole wood are given as shown in Fig. 26 (e)-(h). In these diagrams, the orientation distributions of four crystallographic planes have cylindrical symmetry around the longitudinal axis of wood, but their distribution patterns are quite different each other. In (101) plane, the orientation distribution is described as a single "belt" on the equator [Fig. 26 (e)]. In (10$\bar{1}$) and (002) planes, the distribution "belts" are split into two "belts": the one on the upper hemisphere, and the other on the lower hemisphere [Fig. 26 (f)-(g)]. Although the orientation functions essentially have the same α_3 dependency, it is true that the orientation distribution patterns for these three paratropic reflections are quite different, because the pole distribution density is dependent only upon the variation of α_3 value, and the variation is appeared only around the longitudinal direction. This is the reason why the orientation distribution "belt" is split into two parts for the whole features of orientation distributions of (10$\bar{1}$) and (002) crystallographic planes.

3. Experimentals

3-1. Specimen

Three-dimensional diffraction intensity distributions of (101), (10$\bar{1}$), (002) and (040) planes for cellulose crystallites in opposite, normal and compression wood of a *Pinus densiflora* were measured. These samples were prepared as a plate [20 mm (T) $\times$ 20 mm (L) $\times$ 1 mm (R)] from a tree that had been growing in Kamigamo University Forest, Kyoto University. The Cartesian coordinate system (Fig. 27) was fixed on the sample space in these measurements.

3-2. Instruments

A Rigaku-denki Rotaflex RU-3L was used in these measurements, and a pole figure attachment was set on the goniometer. The line focusing x-ray optical system was applied in these measurements. The measurements were carried out by 2θ-

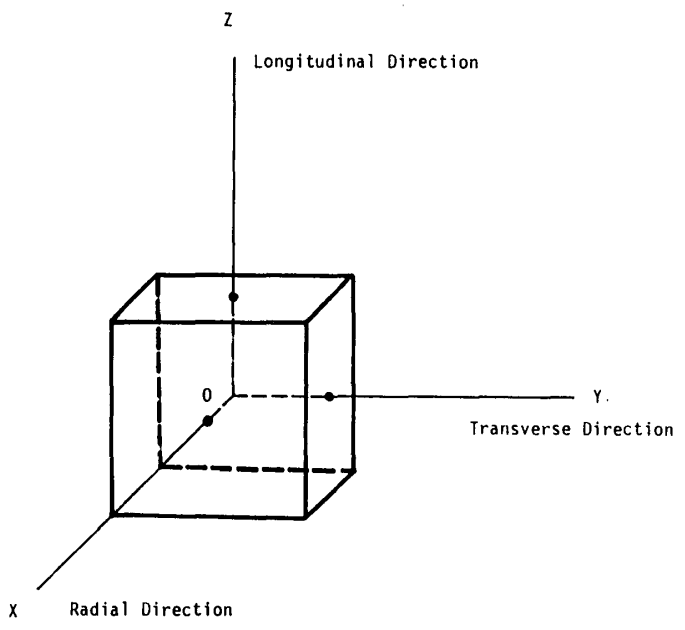

Fig. 27. Cartesian coordinate system fixed on sample space.

scanning by a combination of both transmission and reflection techniques (Tanaka *et al.* 1977) as shown in Table 1.

Table 1. Measurement conditions for x-ray diffraction

Equipment used	Rigaku-denki Rotaflex RU-3L (with Cu target)
Acc. voltage	45 kV
Acc. current	80 mA
Div. slit	1/2 degree
Scat. slit	1/2 degree
Receiv. slit	3/10 mm
Time const.	5 sec
Scan. speed	1/2 degree/minute
Filter	Ni

3-3. Measurements

The 2θ-scanning was carried out for each sample geometry, and the reflection intensities were recorded for each crystallographic plane. The transmission technique was used for the sample geometry $\alpha=0°$ to $\alpha=50°$, and the reflection technique for $\alpha=40°$ to $\alpha=90°$ (Cullity 1956). The line focusing x-ray optical system was used in these measurements to increase the intensity of the diffraction. The correction factors for irradiated volume and absorption were measured experimentally by the use of randomly oriented cellulose sample prepared in the same size and shape used in the measurements. The factors for air scattering and background noise cor-

rections were also experimentally measured. For correction of amorphous scattering in (101), (10$\bar{1}$) and (002) planes, assuming that the line profiles of crystalline scatteing and amorphous scattering were described by Gaussian curves (Eq. 56), and that the total line profile was shown by linear combination of their line profiles, each scattering was separated mathematically from the total scattering with least square method (Sarko 1979). The integral intensities for each crystalline scattering were, then, calculated (Eq. 57).

$$i(\theta)=i_0 \exp\left[-\ln 2\left\{\frac{2(\theta-\theta_0)}{\beta}\right\}^2\right] \tag{56}$$

where $i(\theta)$ is diffraction intensity, i_0 diffraction intensity at $\theta=\theta_0$, β half width for peak profile and θ_0 Bragg angle for peak position.

$$I_{hkl}=\int i(\theta)\,d\theta \tag{57}$$

where I_{hkl} is an integral intensity. For amorphous scattering in the (040) peak regions, tangential lines which contact at two points on the diffraction curves were drawn and the region below these lines was regarded as the amorphous scattering. The diffractions divided in these processes were further refined by approximating their line profiles as Gaussian (Eq. 56), and their integral intensities were also calculated by Eq. (57). The factors for polarization, non-elastic scattering and temperature corrections were not taken into consideration because of their negligibly small contribution to the intensity data. The values of β_0 for (101), (10$\bar{1}$), (002) and (040) peak positions were calculated with the unit cell parameters for ramie cellulose determined by Woodcock *et al.* (1980). The intensity distributions for both transmission and reflection techniques in the region of $\alpha=40°$ to $\alpha=50°$, where the measurements overlapped, were used to determine the scaling factor. In this fashion, the standard three- dimensional intensity distributions based on the transmission technique were obtained. Furthermore, the distributions were converted into probability distributions by Eq. (58), and the total amount of these distributions was normalized as unity on the whole unit sphere.

$$W(\phi,\psi)=\frac{I(\phi,\psi)}{\int_0^{\pi}\int_0^{2\pi} I(\phi,\psi)\sin\phi\,d\psi\,d\phi} \tag{58}$$

where $W(\phi,\psi)$ is a probability function of the orientation distribution, $I(\phi,\psi)$ diffraction intensity distribution, ϕ polar angle against the reference axis (X-axis), and ψ azimuthal angle around the reference axis (X-axis, from the Z-axis). These were regarded as the orientation distributions for the lattice planes of cellulose crystallites in *Pinus densiflora* wood. Three-dimensional orientation distributions were described in the three dimensional orientation probability distributions on the half unit sphere, and were projected stereographically on the two dimensional planes. Due to the

orthogonally bi-axial symmetry prevailing in the orientation distributions of wood cellulose crystallites, the projected distributions were represented in the map of quarter circle.

4. Results and Discussion

Figure 28 shows the three-dimensional orientation distributions of (101), (10$\bar{1}$), (002) and (040) lattice planes in the cellulose crystallites in *Pinus densiflora* wood expressed by probability functions. These figures are represented on the projections on the *Y*-*Z* planes. The point $\phi=0°$ coincides with the direction for the radial axis (*X*-axis), the point at $\phi=90°$ and $\psi=0°$ with the direction for the longitudinal axis (*Z*-axis), and the point at $\phi=90°$ and $\psi=90°$ with the direction for the tangential axis (*Y*-axis). It is noticed that the orientation densities are higher and the distributions are sharper, when the values of the densities (the values of the numerals in the diagrams) are larger. The orientation densities are lower and the distributions are broader when the values are smaller.

In the opposite wood [Fig. 28 (a) to (d)], the orientation of (040) plane normals were more densely populated in the direction of the longitudinal axis and the distribution was not broad. The orientations of (101), (10$\bar{1}$) and (002) plane normals,

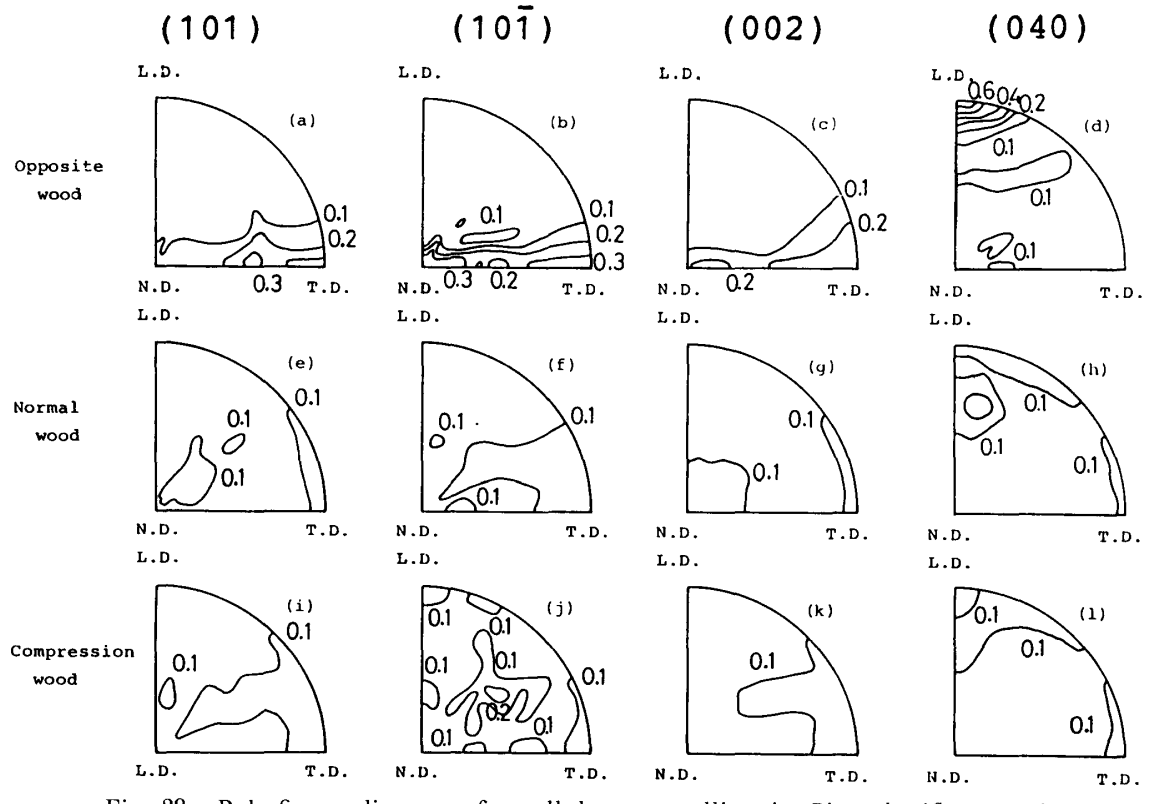

Fig. 28. Pole figure diagrams for cellulose crystallites in *Pinus densiflora* wood expressed by probability functions.

that provide paratropic reflections, laid in the plane perpendicular to the longitudinal axis with higher probability, and their distributions were not broad. These orientation distributions around the longitudinal reference axis were nearly in a uni-axial fashion, in spite of the fact that the opposite wood has a rectangular cross sectional shape of cell walls. Furthermore, all the sidtribution patterns were nearly the same for these three paratropic reflections. Therefore, it can be concluded that the orientation distributions of the cellulose crystallites in the cell walls of tracheids in the opposite wood are nearly uni-axial.

In the normal wood [Fig. 28 (e) to (h)], the location of the maximum points of the orientation distribution densities for the (040) planes [Fig. 28 (h)] reflected the rectangular cross sectional shape of the tracheids. The higher density region at $\phi=90°$ and $\psi=0°$ to $\psi=40°$ means that the cellulose crystallites are more populated in the tangential walls of the tracheids, and the region near $\phi=50°$ to $\phi=80°$ and $\psi=0°$ to $\psi=25°$ corresponds to the cellulose crystallites present in the radial walls. The lower density part in the center of latter region might result from the fact that the orientation distributions of cellulose crystallites in cell walls of the normal wood are spirally oriented along the fibril axis as observed with optical microscope. The region near the tangential axis seems to correspond to the cellulose crystallites present in the ray cells, or primary walls and outer and inner layers of secondary walls of tracheids. These distribution densities were not small, and, therefore, should not be omitted. The orientation distributions of the (101), $(10\bar{1})$ and (002) planes also reflected the cross sectional shape of the tracheids, and were more populated along the tangential and radial axes. The differences of the orientation modes among the (101), $(10\bar{1})$ and (002) planes are not distinct due to some contribution of uni-axial orientation mode around the longitudinal axis. But it should be noticed that the orientation distributions of these paratropic reflections tend to split into two parts. It is, therefore, interpreted that the orientation distributions of cellulose crystallites in the normal wood cell walls have a bi-axial orientation with certain degree of uni-axial orientation mode around the longitudinal axis.

In the compression wood [Fig. 28 (i) to (l)], the orientation distributions of the (040) planes [Fig. 28 (l)] splitted into two regions: one as a ring around the longitudinal axis, and the other nearly along the tangential axis. The former reflects that the cellulose crystallites are present in the round-shape tracheid, and the latter reflects that they are present in the ray cell, or in the primary walls and outer layers of the secondary wall of the tracheid. The paratropic (101), $(10\bar{1})$ and (002) reflections did not show a sharp distribution, and the distribution patterns were not simple. They were irregular along the fibril axis and not cylindrical. The

paratropic reflections were widely distributed on the diagrams, and each distribution pattern was more clearly defined than in the case of the normal wood. From these facts, it is concluded that the otientation mode of cellulose crystallites in the compression wood cell wall are also bi-axial orientation with certain degree of uni-axial orientation mode around the longitudinal axis. The degree of uni-axial orientation features in the compression wood is not so clear as in the case of the normal wood.

The average squared directional cosines for polar and azimuthal angles with the radial axis as the refernce axis were calculated for each crystallographic plane by Eqs. (59) and (60) from the distributions shown in Figure 28.

$$\langle\cos^2\phi\rangle=\int_0^{\pi}\int_0^{2\pi}W(\phi,\psi)\cos^2\phi\sin\phi d\psi d\phi \tag{59}$$

$$\langle\cos^2\psi\rangle=\int_0^{\pi}\int_0^{2\pi}W(\phi,\psi)\cos^2\psi\sin\phi d\psi d\phi \tag{60}$$

The average squared cosines for polar angles with both longtiudinal and tangential axes as the reference axes were also caluculated by Eqs. (61) and (62) (Takahara *et al.* 1968) assuming that no correlations exist between the distributions for polar and azimuthal angles.

$$\langle\cos^2\phi_z\rangle=\langle\cos^2\psi_x\rangle\{1-\langle\cos^2\phi_x\rangle\} \tag{61}$$

$$\langle\cos^2\phi_y\rangle=-\{\langle\cos^2\phi_z\rangle+\langle\cos^2\phi_x\rangle\} \tag{62}$$

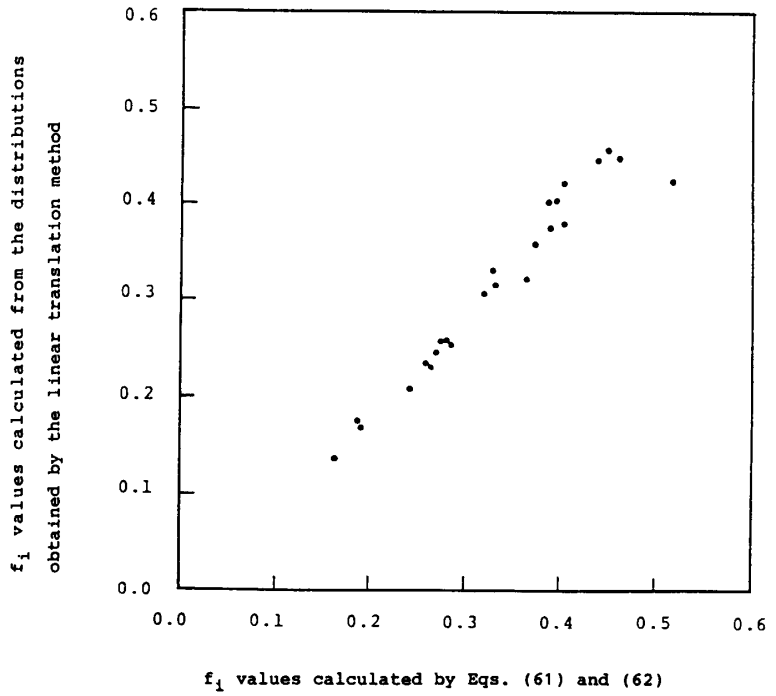

Fig. 29. Relationship between observed and theoretical f_i values.

The assumption applied here can be verified as follows. The orientation distributions with the reference axes of both longitudinal and tangential axes were calculated from the distributions described in Figure 28 using linear translation and two dimensional iterations. The orientation factors, f (for details see later paragraph), can be calculated from the orientation distributions with the reference axes of radial, longitudinal and tangential axes, and these orientation factors were compared each other (Fig. 29).

Table 2. Orientation functions

		$\langle\cos^2\phi_x\rangle$	$\langle\cos^2\phi_y\rangle$	$\langle\cos^2\phi_z\rangle$
Opposite wood	(101)	0.366	0.449	0.185
	($10\bar{1}$)	0.376	0.460	0.161
	(002)	0.293	0.518	0.189
	(040)	0.282	0.281	0.437
Normal wood	(101)	0.367	0.364	0.269
	($10\bar{1}$)	0.355	0.404	0.241
	(002)	0.417	0.327	0.256
	(040)	0.281	0.318	0.401
Compression wood	(101)	0.350	0.389	0.261
	($10\bar{1}$)	0.355	0.372	0.273
	(002)	0.327	0.395	0.278
	(040)	0.283	0.331	0.386

The average squared cosines of polar angles are listed with the three reference axes in Table 2. Figure 30 represents the three-dimensional orientation distribution mode on the equilateral triangular coordinate system devised by Desper *et al.* (1966). In these diagrams the point on the centroid of the triangle corresponds to a random orientation mode in the three-dimensional field, as was mentioned already. Depending upon how far an observed point deviates from the centroid in this equilateral triangular coordinate, the degree of the preferred orientaion can be as represented the average squared cosine.

In the opposite wood, the orientation mode of the (040) planes was nearly in a uni-axial orientation around the longitudinal axis, and the direction of averaged orientation was virtually in the direction of this longitudinal axis. The orientation distributions for the (101), ($10\bar{1}$) and (002) planes, which gave paratropic reflections, had some degree of inclinations toward the tangential axis. This means that the orientation distribution of cellulose crystallites in the opposite wood is of uni-axial type, and there are more cellulose crystallites present in the radial than in the tangential wall.

In the normal wood, the orientation distribution for the (040) planes was also

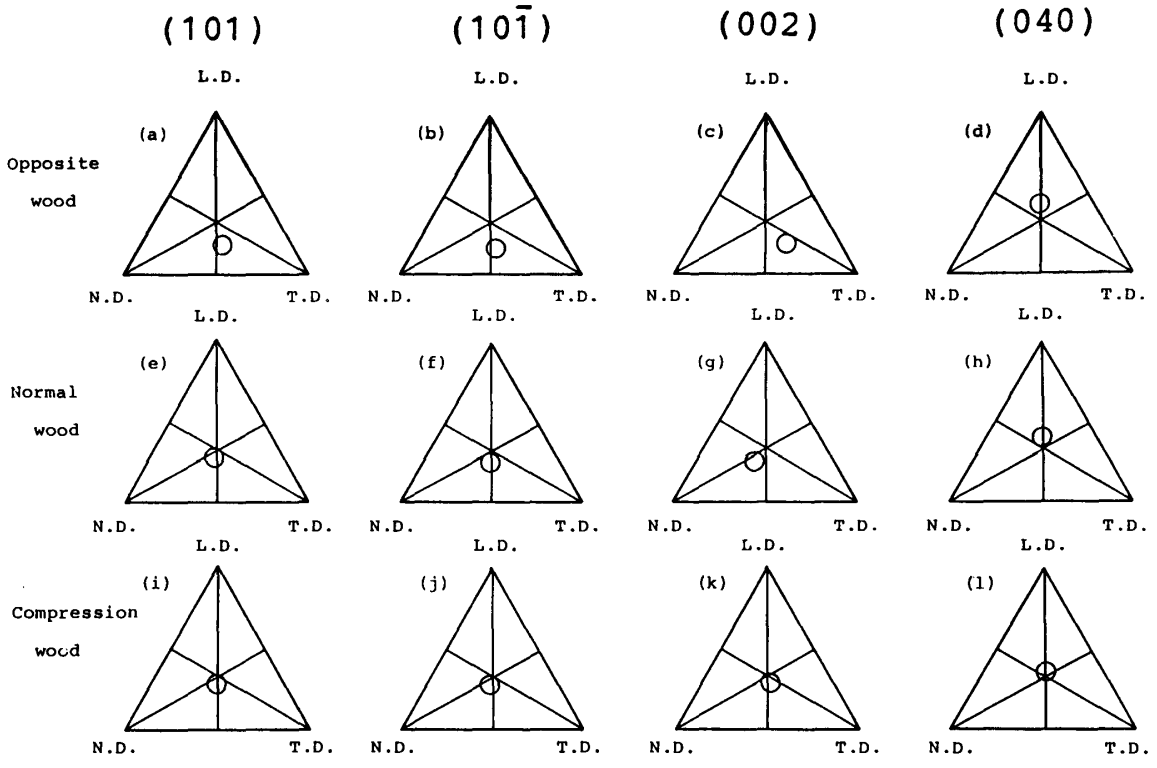

Fig. 30. Equilateral triangular coordinate plots of average directional squared cosines for distributions of cellulose crystallites in *Pinus densiflora* wood.

inclining toward the longitudinal axis, and had nearly uniform averaged orientation, but the degree of inclination toward the longitudinal axis was less than that in the case of the opposite wood. The orientations of the (101), (10$\bar{1}$) and (002) planes had also the distributions nearly in the plane perpendicular to the longitudinal axis, and thier averaged orientation distributions were nearly uniform.

In the compression wood, the orientation distribution of the (040) planes also showed a pattern with some inclination toward the longitudinal axis, but the degree of inclination was less than in the other two types of wood, and it had rather random orientation mode. The distribution pattern is also uniform around the longitudinal axis. The orientation patterns for the (101), (10$\bar{1}$) and (002) planes show also uniform distributions around the longitudinal axis, and their orientation distributions are almost in the plane perpendicular to this axis. The orientation distributions for the compression wood were much broader than those for other two types of woos.

From these results it is understood that the orientation distributions of cellulose crystallites in the direction perpendicular to the longitudinal axis always reflect the cross sectional shape of the tracheids, and their averaged orientations show balanced distributions around the longitudinal axis. These are keeping with the fact that the bulk properties of wood originated by cellulose crystallites are nearly isotropic in the

plane perpendicular to the longitudinal axis. The orientation distributions along the longitudinal axis are all inclining toward this axis, and show some preferred orinetation features. The degree of inclination toward the longitudinal axis increases with the order compression wood<normal wood<opposite wood. The degree of inclination is quantitatively represented in terms of $\langle\cos^2\phi\rangle$. The typical values of $\langle\cos^2\phi\rangle$ are following,

$$\begin{aligned}&\langle\cos^2\phi\rangle \text{ (for perfect perpendicular orientation mode)} = 0.0\\ &\langle\cos^2\phi\rangle \text{ (for random orientation mode)} = 1/3\\ &\langle\cos^2\phi\rangle \text{ (for perfect parallel orientation mode)} = 1.0\end{aligned} \tag{63}$$

Furthermore, the values of $\langle\cos^2\phi\rangle$ can quantitatively represent the anisotropic features of the bulk properties of wood, and they are originated from the properties of cellulose crystallites. However, this representation is not suitable to directly express the orientation mode and the degree of isotropy of the bulk property of wood. Instead, the distribution fucntion is expanded with the spherical harmonics (Sack 1961, Roe *et al.* 1964) and their second moment expressed as Eq. (64) is considered.

$$f=\frac{3\langle\cos^2\phi\rangle-1}{2} \tag{64}$$

Equation (64) is equivalent to the orientation factor defined by Hermans *et al.* (1946). The typical values of f are follows.

$$\begin{aligned}&f \text{ (for a perfect perpendicular orientation)} = -0.5\\ &f \text{ (for a random orientation)} = 0.0\\ &f \text{ (for a perfect parallel orientation)} = 1.0\end{aligned} \tag{65}$$

The Hermans' expression is easier to understand the relation between orientation distribution of crystallites in the sample and the bulk property of the sample.

Table 3. Orientation factors

		f_x	f_y	f_z
Opposite wood	(101)	0.049	0.174	−0.223
	(10$\bar{1}$)	0.069	0.190	−0.259
	(002)	−0.061	0.277	−0.217
	(040)	−0.077	−0.079	0.156
Normal wood	(101)	0.051	0.046	−0.097
	(10$\bar{1}$)	0.033	0.106	−0.139
	(002)	0.126	−0.010	−0.116
	(040)	−0.079	−0.023	0.102
Compression wood	(101)	0.025	0.084	−0.109
	(10$\bar{1}$)	0.033	0.058	−0.091
	(002)	−0.010	0.093	−0.083
	(040)	−0.076	−0.004	0.079

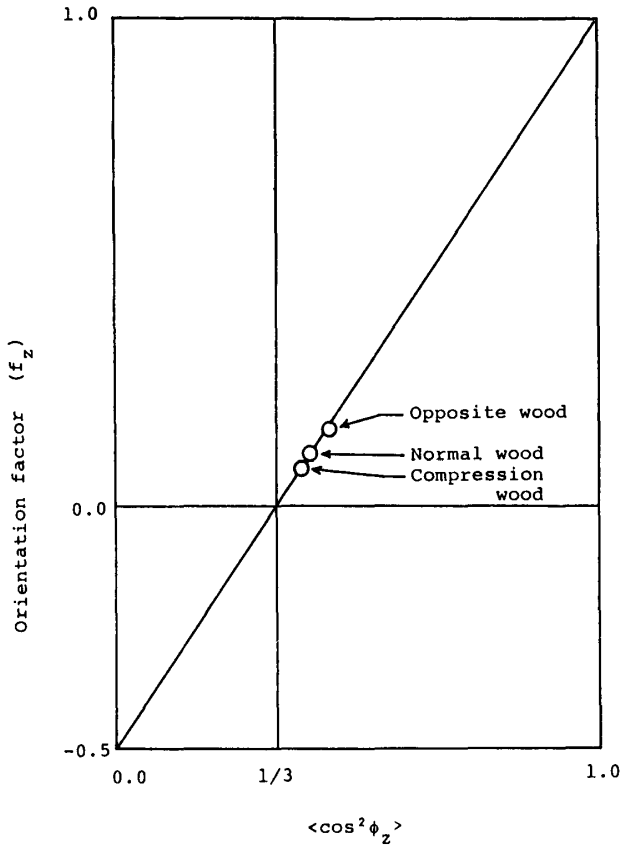

Fig. 31. Relationship between orientation factors and orientation functions.

Orientation factors for *Pinus densiflora* wood are listed in Table 3. The f vs. $\langle\cos^2\phi\rangle$ plots are shown in Fig. 31. They show a linear correlation between values f and $\langle\cos^2\phi\rangle$ as is expected from Eq. (64). Averaged orientation angles $\langle\phi\rangle$ which are independent of the values $\langle\cos^2\phi\rangle$, were also calculated by Eq. (66).

$$\langle\phi\rangle=2\int_0^{\pi/2}\int_0^{2\pi}W(\phi,\psi)\phi\sin\phi d\psi d\phi \qquad (66)$$

Figure 32 shows the relationship between f and $\langle\phi\rangle$ values, which is a simple correlation. The $\langle\phi\rangle$ value shows an averaged inclination of a certain direction of a cellulose crystallite in wood against a reference axis, and directly corresponds with an averaged fibril angle, and the f value, defined by Hermans *et al.* (1946), in an index which reflects an anisotropy of bulk property of wood, such as mechanical, optical or electrical one. Therefore, the correlation described in Fig. 32 shows that bulk property of wood reflects its anatomy. This means that the wood property can be explained by the wood structure, especially the orientation distribution of cellulose crystallites.

From Fig. 30, it is clear that the orientation mode of cellulose crystallites in wood are closely related to the variation of cell structure in wood, and more so to the variation in orientation factors. Little variation for the orientation mode was noticed

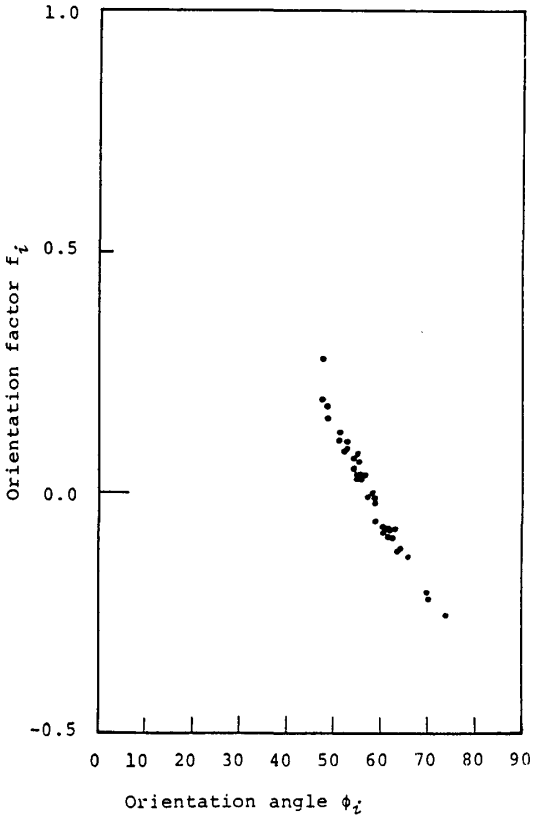

Fig. 32. Relationship between orientation factors and averaged orientation angles.

in the orientation distributions on the horizontal plane. It is, therefore, believed that one of the factors affecting the orientation distribution of cellulose crystallites in the horizontal plane is the structure of the wood cells. On the contrary, much variation of the preferred orientation modes was detected in the vertical direction, and this corresponded to the differences of the anatomy among compression, normal and opposite woods. This suggests the existence of some kinds of physical forces in the tree, as an analogy of synthetic polymers. These forces might be regulated by the growing condition of tree. One of these forces, probably the internal stress, is concerned with the orientation mechanism of cellulose crystallites. From the hypothesis published by Wardrop (1964), it is considered that the magnitude of this stress in wood increases with the order compression wood<normal wood<opposite wood. The order of the values of the orientation factors for cellulose crystallites in *Pinus densiflora* wood as well as the size of the crystallites in the wood cell walls (Tanaka *et al.* 1981) is correlated with that of the magnitude of the internal stress. This suggests that at least phenomenally there exist some relations between the orientation of cellulose crystallites and the internal stress in the wood cell walls. It is, therefore, likely that one of the factors controlling the orientation of cellulose crystallites in

wood is a uni-axial stretching caused by this internal stress.

5. Summary

The three dimensional orientation distributions of cellulose crystallites in opposite, normal and compression wood of a *Pinus densiflora* were quantitatively evaluated by the mehtod of pole figure analysis. The pole figures were described for (101), ($10\bar{1}$), (002) and (040) crystallographic planes of cellulose crystallites. From these diagrams, the orientation modes of cellulose crystallites in the wood cell walls were remarkably different with the variation of compression, normal and opposite woods, as well as the fibrilar angles. It was found that the orientation distribution of cellulose crystallites in the wood for the polar angles is independent upon that for azimuthal angles. The orientation modes of cellulose crystallites in the wood are bi-axial with some certain degree of uni-axial mode. The fraction of uniaxially oriented cellulose crystallites was in the increasing order of compression, normal and opposite wood. The larger the fraction values are, the smaller fibril angle to the longitudinal axis is expected. From these observations and the characteristics of wood cellulose described in chapter 3, a uni-axial stretching mechanism is considered as an orientation mechanism of cellulose crystallites in the wood cell wall, as an analogy of synthetic polymers: the orientation of cellulose crystallites in the wood cell walls is not in the biosynthesis stage of cellulose molecules, but it is carred out after the cellulose molecules are synthesized.

CONCLUSIONS

The fiber textures and the characteristics of wood cellulose were quantitatively discussed by correlating the ultra-fine structure of wood to its bulk properties. The studies on these fields have been only limited in qualitative basis, and they were discussed based on the investigators' intuition and bias. To be more quantitative, a physico-chemical approach such as the pole figure analysis, which had been successfully applied in the study on the textures of metals, was modified and applied in this study: first the whole features of orientation distributions of celluloses crystallites in wood was observed, and secondly the orientations was quantitatively evaluated.

The procedures of the pole figure analysis was modified so as to make applicable for the orientation study of cellulose crystallites, and *Valonia* cellulose was studied as a model of cellulose. The precise orientational features of *Valonia* cellulose was obtained by the modified pole figure method. The orientational mode of *Valonia* cellulose crystallites showed a double orientation (uniplanar-axial) in which crystallites were mutually crossed almost perpendicularly. The crystallographic planes under planar orientation mode were all ($2\bar{2}0$) planes, and it was experimentally found

that the direction of their distribution maxima was precisely coincided with the plane normal of the sample surface. The planar orientation concept of *Valonia* cellulose proposed by R.D. Preston (1951), who derived from insufficient x-ray fiber diagrams of *Valonia* cell walls, was supported by these pole figures of *Valonia* cellulose. Furthermore, two mutually antiparallel arrays of cellulose crystallites in each orientation unit of microfibrils were also found experimentally. The third minor orientation of cellulose crystallites in *Valonia* cell walls, which was suggested by R.D. Preston (1951), was also observed, even though it constituted only small portion of cellulose crystallites. The modified pole figure method derived here was found to be useful for the measurement of the orientation distributions of natural polymer crystallites such as cellulose.

Before the application of the modified pole figure method to the orientation study of *Pinus densiflora* wood cellulose, the celluloses in compression, normal and opposite woods were characterized. From the measurement of molecular weight of cellulose, the degree of crystallinity of cellulose, and the orientations and size of cellulose crystallites in wood, the following results were obtained.

(1) The degree of polymerization of celluloses in the wood is not different among all three different woods.

(2) The degree of crystallinity (*DC*) of cellulose among three different wood is as follows.

Cellulose in opposite wood	50%–60%
Cellulose in normal wood	about 50%
Cellulose in oompression wood	45%–50%

From the hypothesis proposed by Wardrop (1964), these values were expected to have close relations with the magnitudes of the internal stress of wood. The *DC* values were also found to decrease with the increase of the height above the ground.

(3) The degree of orientation of cellulose crystallites along the longitudinal direction of wood was in the order of opposite>normal>compression among three different woods. The degree of crystallinity was also expected to have close relations with the magnitudes of the internal stress of wood.

(4) The crystalline size of wood cellulose in the transverse direction was found to be nearly constant among three different woods, while those in the longitudinal direction (crystallite length) have large difference among three The crystalline length of the cellulose crystallites in the opposite wood was much longer than that in the compression wood. The length of crystallites in the opposite wood had correlations with the height above the ground, although that in the compression wood was nearly constant.

From above discussion, it is considered that the characteristics of wood cellulose

have close correlations with the internal stress during the tree growth.

The three-dimensional orientation distributions of cellulose crystallites in the wood were measured, and their orientations were evaluated. The correlations between the orientation of cellulose crystallites in woods and their bulk properties were also discussed. The modified pole figure method described already was further refined, because many defects were noticed when the method was directly applied to the orientation study of the wood cellulose. When this refined and modified pole figure method was applied to the orientation study of the wood cellulose, the precise orientational evaluation of the wood cellulose became possible. The orientation modes of cellulose crystallites in three anatomically different *Pinus densiflora* woods were found to be different one another as well as their fibrilar angles. Accoridng to the hypothesis proposed by Wardrop (1964), an observation would show good a correlation between the orientation of wood cellulose crystallites and the order of the magnitudes of internal stress in the wood. From these discussion, a uniaxial-stretching mechanism could be considered as an orientation mechanism of cellulose crystallites in the wood cell wall. From the correlations between the orientation of cellulose crystallites in the wood and the anatomy of the wood, ti was found that the bulk properties of the wood was greatly influenced by the latter.

The refined and modified pole figure method also gives an answer to the question whether the cellulose crystallites in the wood cell walls are axially or planarly oriented. It was found that the orientation mode of cellulose crystallites in the wood cell walls was neither entirely axial nor planar, but in the inermediate between axial and planar orientation modes.

From above discussions, it became possible to give a clear answer to the question whether the wood cellulose was a member of generally occurring natural celluloses or not. This question originally arose from the observations that the orientation of the wood cellulose might be quite different from those of gerneally occurring natural celluloses. The difference of the orientation modes between the wood cellulose and the generally occurring other natural celluloses are not the essential one, and that noticed are only secondary effect derived as a result of the orientation mechanism of cellulose crystallites in the wood. Thus it was confirmed that the wood cellulose in one kind of the naturally occurring celluloses.

ACKNOWLEDGMENTS

This article is partly based on the studies carried out by the author at Department of Wood Scinece and Technology, Faculty of Agriculture, Kyoto University, Kyoto, Japan, and Research Section of Wood Chemistry, Wood Research Institute, Kyoto University, Uji-city, Kyoto, Japan, from 1973 to 1984, under the auspices of Professor

Hajime Okamoto, and Professor Tetsuo Koshijima, to whom the author wishes to express his gratitude. He wishes to express his gratitude to Professor Keizo Okamura, Department of Wood Science and Technology, Faculty of Agriculture, Kyoto University, for his leadings and suggestions. He wishes to express his gratitude to Professor Anatole Sarko, Department of Chemistry, College of Environmental Science and Forestry, State University of New York, Syracuse, New York, USA, for his permission to use his computer programs and his useful suggestions and discussions. He wishes to express his gratitude to Dr. Yasutsugu Yokohama, Tokyo University of Education, who offered his *Valonia* samples, and Dr. Masaru Matsuo, Nara Women's Universtiy, who instructed the pole figure techniques.

The calculation of orientation functions and factors was carried out with the use of the Computer System at Data Processing Center, Kyoto University.

These studies were partly supported by Scientific Research Funds No. 56308011, No. 57360010 and No. 58360017 of Ministry of Education, Science and Culture. The micro computer system used in the studies for the data processing of the crude x-ray diffraction intensity data was purchased by the support of Scientific Research Funds No. 57760132 and No. 58760125 of Ministry of Education, Science and Culture.

REFERENCES

L.E. ALEXANDER: *X-ray Diffraction Methods in Ploymer Science*, John Wiley & Sons Inc., New York, USA (1969).
W.J. ALEXANDER and R.L. MITCHELL: Anal. Chem., **21**, 1497 (1949).
W.T. ASTBURY and R.D. PRESTON: Proc. R. Soc., **B129**, 54 (1940).
A. BOURRET, H. CHANZY and R. LAZARO: Biopolymers, **11**, 893 (1972).
B.D. CULLITY: *Elements of X-ray Diffraction*, Addison-Wesley Publishing Company Inc., Reading Massachusetts, USA (1956).
C.R. DESPER and R.S. STEIN: J. Appl. Phys., **37**, 3990 (1966).
E. FREI and R.D. PRESTON: Proc. R. Soc. London, **B154**, 70 (1961).
A. FREY-WYSSLING and K. MÜHLETHALER: Fortschr. Chemie Org. Naturstoffe, **8**, 1 (1951).
M. FUJII, J. AZUMA, F. TANAKA and T. KOSHIJIMA: Wood Research, No. 68, 8 (1982).
D.A.I. GORING and T.E. TIMELL: Svensk Paperstidn., **63**, 524 (1960).
D.A.I. GORING and T.E. TIMELL: Tappi, **45**, 454 (1962).
H. HARADA *et al.*: Bulletin Govt. Forest Sta., No. 104 (1958).
C.J. HEFFELFINGER and R.L. BURTON: J. Polym. Sci., **47**, 289 (1960).
J.J. HERMANS, P.H. HERMANS, D. VERMAAS and A. WEIDINGER: Rec. Trav. Chim., **65**, 427 (1946).
G. HONJO and M. WATANABE: Nature, **181**, 326 (1958).
M. HORIO, K. KOBAYASHI and T. KONDO: Text. Res. J., **17**, 264 (1947).
M. HORIO: Text. Res. J., **20**, 373 (1950).
R. HOSEMANN: J. Polym. Sci., Part C, No. 20, 1 (1967).
G. JAYME and H. KNOLLE: Das Papier, **18**, 249 (1964).
F.W. JONES: Proc. R. Soc., **166**, 16 (1938).
W. KLAUDITZ: Holzforschung, **11**, 110 (1957).
D.R. KREGER: Nature, **180**, 914 (1957).

C.H. LINDSLEY and M. FRANK: Ind. Eng. Chem., **45**, 2491 (1953).
M. MATSUO, S. NOMURA and H. KAWAI: J. Polym. Sci., Polym. Phys. Ed., **11**, 2057 (1973).
N. MIGITA, Y. YONEZAWA and T. KONDO Ed.: *Mokuzai-kagaku*, Kyoritsu Publishing Company Inc., Tokyo, Japan (1968).
S.M. MUKHERJEE and J. WOODS: Biochim. Biophys. Acta, **10**, 499 (1953).
E. NICOLAI and A. FREY-WYSSLING: Protoplasma, **30**, 401 (1938).
I.A. NIEDUSZYNSKI and E.D.T. ATKINES: Biochim. Biophys. Acta, **222**, 109 (1970).
L.S. NIELSEN: *Mechanical Properties of Ploymers and Composites*, M. Decker, New York, USA (1975).
I. NITTA Ed.: *X-Sen Kessho Gaku*, 4th Ed., Maruzen Company Inc., Tokyo, Japan (1973).
S. NOMURA, S. KAWABATA, H. KAWAI, Y. YAMAGUCHI, A. FUKUSHIMA and H. TAKAHARA: J. Ploym. Sci., Part A-2, **7**, 325 (1969).
M. NORIMOTO, T. OHGAMA, T. ONO and F. TANAKA: J. Soc. Rheology, Japan, **9**, 169 (1981).
T. OHGAMA: Dr. Agr. Thesis, Faculty of Agriculture, Kyoto University (1975).
T. OKANO: Mokuzai Gakkaishi, **18**, 583 (1972).
F. ONAKA: Wood Research, No. 1, 1 (1949).
P.R. PINNOCK and I.M. WARD: Brit. J. Appl. Phys., **17**, 575 (1966).
R.D. PRESTON and W.T. ASTBURY: Proc. Roy. Soc., **B122**, 76 (1937).
R.D. PRESTON: Disc. Faraday Soc., **11**, 165 (1951).
R.D. PRESTON: *Molecular Architecture of Plant Cell Walls*, Chapman & Hall Ltd., London (1952).
R.D. PRESTON: *The Physical Biology of Plant Cell Walls*, Chapman & Hall Ltd., London (1974).
J.-F. REVOL, C. GANCET and D.A.I. GORING: Wood Science, **14**, 120. (1982).
R.J. ROE and W.R. KRIGBAUM: J. Chem. Phys., **40**, 2608 (1964).
R.A. SACK: J. Polym. Sci., **54**, 543 (1961).
A. SARKO: Computer Program "LSQ", version 1979, State University of New York, Syracuse, New York 13210, USA (1979).
P. SCHERRER: Göttingen Nachr., 98 (1918).
K. SHIMAJI, S. SUDOU and H. HARADA: *Mokuzai no Soshiki*, Morikita Publishing Company Inc., Tokyo, Japan (1976).
L.G. SCHULZ: J. Appl. Phys., **20**, 1033 (1949a).
L.G. SCHULZ: J. Appl. Phys., **20**, 1030 (1949b).
J. SCHURZ: Phyton, **5**, 53 (1955).
W.A. SISSON: J. Phys. Chem., **40**, 343 (1936).
O.L. SPONSLER: Protoplasma, **12**, 241 (1931).
T. TAKAHASHI: Sen-i Gakkaishi, **25**, 80 (1969).
H. TAKAHARA and H. KAWAI: Sen-i Gakkaishi, Sen-i to Kogyo, **21**, No.5S, S120 (1965).
H. TAKAHARA, S. NOMURA, H. KAWAI, Y. YAMAGUCHI, K. OKAZAKI and A. FUKUSHIMA: J. Polym. Sci., Part A-2, **6**, 197 (1968).
H. TAKAHARA: Dr. Eng. Thesis, Faculty of Engineering, Kyoto University (1969).
H. TAKAHARA, H. KAWAI, Y. YAMAGUCHI and A. FUKUSHIMA: Sen-i Gakkaishi, **25**, 60 (1969).
M. TAKAI, Y. TSUDA, J. HAYASHI and S. WATANABE: J. Polym. Sci., Polym. Lett. Ed., **12**, 221 (1974).
M. TAKAI, Y. TSUDA, J. HAYASHI and S. WATANABE: Polymer J., **7**, 157 (1975).
F. TANAKA and K. OKAMURA: Abstract Presented at the 24th Annual Meeting of Japan Wood Research Society, Tokyo, in April (1974).
F. TANAKA and K. OKAMURA: J. Polym. Sci., Polym. Phys. Ed., **15**, 897 (1977).
F. TANAKA, T. TAKAKI, K. OKAMURA and T. KOSHIJIMA: Wood Research, No. 66, 17 (1980).
F. TANAKA T. KOSHIJIMA and K. OKAMURA: Wood Sci. & Technol., **15**, 265 (1981).
F. TANAKA and T. KOSHIJIMA: Mokuzai Gakkaishi, **29**, 1 (1983).
F. TANAKA and T. KOSHIJIMA: Wood Sci. & Technol., **18**, 177 (1984).
B.K. VAINSHTEIN: *Difraktsiya Rentgenovykh Luchey na Tsepnykh Molekulakh*, Izdatel'stvo Akademii Nauk SSSR, Moscow, USSR (1963).
I.M. WARD: Proc. Phys. Soc., **80**, 1176 (1962).

A.B. WARDROP: Holzforschung, **8**, 12 (1954).
A.B. WARDROP: The Reaction Anatomy of Arborescent Angiosperms, In: *The Formation of Wood in Forest Trees,* Zimmermann, M.H. Ed., Academic Press, New York, USA (1964).
Z.W. WILCHINSKY: J. Appl. Phys., **30**, 792 (1956).
Z.W. WILCHINSKY: J. Appl. Phys., **31**, 1969 (1960).
C. WOODCOCK and A. SARKO: Macromolecules, **13**, 1183 (1980).